Aspects of Thermography for Non-Destructive Testing in Mechanical Maintenance

by

Bandile Jama

Dissertation submitted in partial fulfilment of the

requirements for the degree

Masters of Engineering: Mechanical Engineering

Supervisor : Prof Jasson Gryzagoridis

Co-supervisor : Mr Graham Wilson

Bellville

2017-11-07

CPUT copyright information

The dissertation may not be published either in part (in scholarly, scientific or technical journals), or as a whole (as a monograph), unless permission has been obtained from the University.

DECLARATION

I, **Bandile Jama**, declare that the contents of this dissertation represent my own unaided work, and that the dissertation has not previously been submitted for academic examination towards any qualification. Furthermore, it represents my own opinions and not necessarily those of the Cape Peninsula University of Technology.

(Signature of student) Date: 2017-11-07

ABSTRACT

Infrared thermography (IRT) is a non-contacting, non-destructive testing (NDT) technique that provides relatively fast results from inspections; for example, in the detection of defects in engineering components and in systems' condition monitoring. This study examines the use and possible effectiveness of infrared thermography for the detection of faults and defects in just a few aspects that one encounters in the vast mechanical maintenance arena. The study discusses three aspects of infrared thermography, namely internal leaks inspections using passive infrared thermography, pulse thermography and induction thermography both active IRT NDT techniques for the detection of subsurface and surface defects.

The promising results that were obtained by performing an experiment in the laboratory using a model fluid handling pipe network, with three isolation valves connected in parallel, encouraged performing inspections in an operating power plant, where it was suspected that there were leaks from safety and drain isolation valves. In both situations, the results were obtained in a short period of time and indicated that passive infrared thermography can detect internal leaks in pipe networks.

Pulsed thermography is an active non-contacting non-destructive testing technique used to detect subsurface defects in monolithic materials and delamination's in composites. In the particular experiment that was performed pulse thermography was benchmarked with the conventional technique of ultrasound testing. PVC, stainless steel and mild steel specimens manufactured with flat bottom holes (as models of subsurface defects) were subjected to pulse thermography. The time duration to detect the presence of a defect represented by a temperature contrast or a hot spot on the specimen's surface was approximately a couple of seconds following the thermal excitation. No further characterization of the defect was possible with the technique. In contrast when using the ultrasound testing technique to test the specimens, it took considerable time to detect the defects, however, data in terms of size and depth beneath the surface became available thus enabling their full characterization.

In this study, the use of induction thermography as an alternative to the conventional non-destructive techniques of magnetic particle and dye penetration inspections for the detection of surface defects was attempted. Experiments using induction thermography, on metallic electromagnetic specimens were performed, in the laboratory as well as on components obtained from the power plant. 304L stainless steel pipe specimen, an HP turbine stud and a CV-joint with natural surface defects (cracks) were subjected to induction thermography

conditions for a short duration. The results delineated the presence of cracks as a solid line with higher contrast compared to other areas of the specimen. In comparison with MPI and DPI, the technique could reveal more defects within a short period of time and may be considered as a preferable NDT technique for large surface inspections as per results obtained from 304L stainless steel specimen.

The results from this study suggest that infrared thermography is a non-destructive technique that can be utilized with different degrees of effectiveness in the mechanical maintenance arena where NDT techniques such as UT, MPI, and DPI have been, by tradition, employed in the past.

Keywords: Infrared Thermography, Pulse Thermography, Induction thermography, defects, UT, MPI, DPI.

ACKNOWLEDGEMENT

I wish to thank:

- The **Lord Jesus** who granted me wisdom, knowledge and understanding, and gave me courage and passion to pursue and complete this study.
- **Amanda Jama** my wife, for her regular support and encouragement towards the completion of this study.
- **Prof. Jasson Gryzagoridis** my principal supervisor, for his professional guidance, motivation and exceptional feedback throughout this study.
- **Graham Wilson "Gra"** my co-supervisor for his words of encouragement and immense knowledge of non-destructive testing and the skills he transferred to me during experiments studies.
- **Zain George**, for his continuous support and availing the NDT lab for me to perform experiments.
- **Prof Graham Oliver**, for his guidance throughout my Master degree program.
- **Angelo Force and his team**, for continuously allowing me to use their infrared camera FLIR T640 throughout the studies.
- **Koeberg Machine Shop Team**, for assisting me with the preparation of specimens.
- **NASA**, for supplying specimens with natural defects from in-service applications.

DEDICATION

Dedicated to my beautiful wife Amanda Jama

And our son Iminathi Jama

I thank you for your love and patience

CONTENT

ABSTRACT ..... **I**

ACKNOWLEDGEMENT ..... **III**

DEDICATION ..... **IV**

CONTENT ..... **V**

LIST OF FIGURES ..... **VIII**

LIST OF TABLES ..... **XI**

GLOSSARY ..... **XII**

CHAPTER 1: INTRODUCTION **1**

1.1 Infrared Thermography 1

1.2 Internal Leaks 2

1.3 Non-Destructive Evaluation of Plant's Components 6

1.4 Main Objectives 8

1.5 Organisation of the Project 8

CHAPTER 2: LITERATURE REVIEW **9**

2.1 Infrared Thermography 9

2.2 Passive Thermography 11

2.2.1 Internal Leak Inspection Passive thermography 12

2.3 Active Thermography 12

2.3.1 Pulsed Thermography 12

2.3.2 Long Pulse Thermography 14

2.3.3 Induction Thermography 15

2.3.4 Lock-in Thermography 16

2.3.5 Ultrasound Thermography 18

2.3.6 Post Processing Methods 19

2.4 Conventional NDT Techniques 19

2.4.1 Magnetic Particle Inspection 19

2.4.2 Dye Penetration Inspection 21

2.4.3 Ultrasound Testing 22

CHAPTER 3: EXPERIMENTAL METHODOLOGY 24

3.1 Introduction 24

3.2 Internal Leak Detection Methodology 25

3.2.1 Experimental Procedure with the Model 26

3.2.2 Laboratory (Model's) Experimental Results 27

3.2.3 Leak detection across Isolation Valves in the Power Plant 28

3.2.4 Results of Internal Leaks through Isolation Valves 29

3.2.5 Leak detection across Safety Valves 30

3.2.6 Results of Internal Leaks through Safety Valves 31

3.3 Pulse Thermography 32

3.3.1 Experimental Procedure of Pulse Thermography 34

3.3.2 Experimental Results 34

3.3.3 Ultrasonic Testing 36

3.3.4 Experimental Procedure of Ultrasound Test 36

3.3.5 Ultrasound Testing Results 38

3.4 Induction Thermography Methodology 41

3.4.1 Research Methodology 43

3.4.2 Experimental Results 44

3.4.3 Magnetic Particle Testing Methodology 46

3.4.4 Results of Magnetic Particle Inspection 46

3.4.5 Dye Penetration Inspection 47

3.4.6 Results of Dye Particle Inspection 48

CHAPTER 4: DISCUSSION AND CONCLUSIONS 50

4.1 Introduction 50

4.2 Internal Leak Inspection 50

4.3 Pulse Thermography 50

4.4 Magnetic Particle Inspection 52

4.5 Dye Penetrant Inspection 52

4.6 Ultrasound Testing 52

4.6.1 Comparison between Pulse thermography and Ultrasound Testing 52

4.7 Induction Thermography 53

4.7.1 Comparison between Induction Thermography and MPI 53

4.7.2 Comparison between Induction Thermography and DPI 54

4.8 Conclusion 54

4.8.1 Future Work 55

APPENDICES 56

Appendix A. Infrared Camera 56

Appendix B. Dimensions and material used to manufacture the FHS 57

Appendix C. Procedure to measure the emissivity 58

Appendix D. Calibration of Kraukramer UT machine using V1 block 59

Appendix F. Induction Thermography Comparison Images 60

BIBLIOGRAPHY 63

LIST OF FIGURES

Figure 1-1. Effects of internal leaks 2

Figure 1-2. Typical schematic diagram of a Pipe network with isolation 3

Figure 1-3. Plant configuration of parallel isolation valves 4

Figure 1-4. Plant configuration of safety valves and discharge pipes 5

Figure 1-5. Schematic diagram of the Pressure relief 5

Figure 1-6. Wheel hub results, thermography results on the left, ... 7

Figure 2-1. Plankian Curves for blackbody emissions at various temperatures, ... 10

Figure 2-2. An in-service pump coupled to its motor (normal image) 11

Figure 2-3. Thermal profile of the in-service pump shown in figure 2.2 11

Figure 2-4. Pulse thermography set up 13

Figure 2-5. Trapped heat flows around the defect 14

Figure 2-6. Induction heating Thermography principle 15

Figure 2-7. Penetration depth vs Frequency for 304L Stainless steel 16

Figure 2-8. Typical setup for lock-in thermography 17

Figure 2-9 Ultrasound Thermography set-up 18

Figure 2-10. Demonstration of MPI during inspection 20

Figure 2-11. Indication of defect using DPI 21

Figure 2-12. Ultrasound testing principle 23

Figure 3-1. FLIR T640 Infrared Camera 24

Figure 3-2. Set up of internal leak inspection using IRT 25

Figure 3-3. Fluid handling system mounted on wooden plinth 26

Figure 3-4. Fluid handling model with valve A cracked open 27

Figure 3-5. Thermal image of model's pipe network before experiment 27

Figure 3-6. Demonstration of system without internal leaks 28

Figure 3-7. Demonstration of internal leak through valve A 28

Figure 3-8. Drain system without internal leaks 29
Figure 3-9. Drain system A with internal leak 29
Figure 3-10. Drain system B with double isolation leaking 30
Figure 3-11. Drain system B with internal leak 30
Figure 3-12. Discharge pipe A results 31
Figure 3-13. Discharge pipe B results 31
Figure 3-14. Discharge pipe C results 32
Figure 3-15. Schematic of the experimental setup of pulse thermography 33
Figure 3-16. Geometry of the test specimen (units in mm) 33
Figure 3-17. Illustration of equipment used during pulse thermography 34
Figure 3-18. Rear view of the specimen with machined defects 35
Figure 3-19. PVC specimen's results 35
Figure 3-20. Stainless Steel specimen's results 35
Figure 3-21. Mild steel specimen's results 35
Figure 3-22. Ultrasound inspection set-up 36
Figure 3-23. Alphabetic Identification of FBH in figure 3-16 37
Figure 3-24. Calibrated Kraukramer Machine 37
Figure 3-25. Echo of the PVC specimen's subsurface defects 38
Figure 3-26. Echo of the Stainless steel specimen's subsurface defects 39
Figure 3-27. Echo of the Mild steel specimen's subsurface defects 40
Figure 3-28. Schematic diagram of Induction Thermography 41
Figure 3-29. Typical 304L stainless steel test piece 42
Figure 3-30. Turbine's stud specimen 42
Figure 3-31. CV-joint 42
Figure 3-32. Coil used for CV-joint inspection 43
Figure 3-33. Typical experimental setup for Induction Thermography 44
Figure 3-34. 304L stainless steel after excitation 45
Figure 3-35. Results of M80 HP turbine's studs after excitation 45

Figure 3-36. Results of CV-joint after excitation 45

Figure 3-37. Experimental set-up of MPI with the turbine's stud 46

Figure 3-38. Turbine stud specimen 47

Figure 3-39. CV-joint from service 47

Figure 3-40. DPI results from the 304L stainless steel test piece 48

Figure 3-41. DPI results from the HP-turbine's stud specimen 48

Figure 3-42. DPI results from the CV-joint 49

Figure B-1. Dimensions of the model system 51

Figure F-1. 304L Stainless Steel Comparison Results 60

Figure F-2. M80 HP Turbine Stud Comparison Results 61

Figure F-3. CV-Joint Comparison Results 62

LIST OF TABLES

Table 3-1. PVC specimen's Ultrasound results 38

Table 3-2. Stainless steel specimen's Ultrasound results..... 39

Table 3-3. Mild steel specimen's Ultrasound testing..... 40

Table 4-1. Material properties of the specimens used in this study..... 51

Table A-1. Infrared Camera Specifications..... 56

Table B-1. Material to manufacture the FHS 57

GLOSSARY

Abbreviations	Definition
AC	Alternating Current
AEP	American Electric Power
CV-joint	Constant Velocity Joint
DC	Direct Current
DPI	Dye Penetration Inspection
FBH	Flat Bottom Hole
FHS	Fluid Handling System
HP turbine	High Pressure Turbine
IR	Infrared Radiation
IRT	Infrared Thermography
MIN	Minute (s)
MPI	Magnetic Particle Inspection
NDE	Non Destructive Evaluation
NDT	Non Destructive Testing
PTFE	Polytetrafluoroethylene
PVC	Polyvinyl Chloride
SCB	Standard Calibration Block
SCC	Stress Corrosion Cracking
UT	Ultrasound Testing
VT	Visual Inspection
WCP	White Contrast Powder

Variables

T_{obj} Object absolute temperature.....$|^0C|$

Q_{obj} Electromagnetic energy released by an object.....$|J|$

$Q_{blackbodyj}$ Electromagnetic energy released by blackbody.....$|J|$

T Temperature.....$|^0C|$

k Thermal conductivity..... $|Wm^{-1}.K^{-1}|$

t	Time	$\lvert s \rvert$
e	Thermal effusivity	$\lvert Ws^{1/2}.m^{-2}K^{-1} \rvert$
c_p	Specific heat	$\lvert Jkg^{-1}.K^{-1} \rvert$
T_0	Initial temperature	$\lvert {}^0C \rvert$
T_C	Thermal contrast	$\lvert K \rvert$
d	diameter of flat bottom hole	$\lvert m \rvert$
D	Depth of flat bottom hole	$\lvert m \rvert$
f	Frequency	$\lvert Hz \rvert$
J	Current density	$\lvert A.m^{-2} \rvert$
E	Electric field intensity	$\lvert N.C^{-1} \rvert$

Greek letters

ε_{obj}	Emissivity	$\lvert - \rvert$
δ	Penetration depth	$\lvert m \rvert$
σ	Stefan Boltzmann	$\lvert W.m^{-2} \rvert$
θ	Angle	$\lvert {}^0 \rvert$
ρ	Density	$\lvert kg.m^3 \rvert$
μ	Permeability	$\lvert Hz.m^{-1} \rvert$
α	Thermal diffusivity	$\lvert m^2.s^{-1} \rvert$
λ	Wavelength	$\lvert m \rvert$

CHAPTER 1: INTRODUCTION

1.1 Infrared Thermography

Infrared thermography (IRT) is considered to be a useful non-contacting non-destructive tool that has not yet met its full potential as a non-destructive testing (NDT) technique in the mechanical maintenance arena. Unlike the current situation in electrical engineering where IRT is extensively used to monitor and find faulty termination in high power electric circuits, identify problems in electric switchgear and locate overloaded circuit breakers in a power panel [1]. In mechanical maintenance, the IRT technique is mainly used for condition monitoring of rotating equipment such as the degradation of bearings and excessive friction on sliding surfaces such as belts and pulleys, clutches and brake slippage [2].

IRT is a technique used to capture and process thermal information from equipment that radiates electromagnetic energy [2]. It is a technique that processes the invisible thermal profile of any object to visible thermal images. This technique applies to all objects that have the temperature above absolute zero degrees, Kelvin, since these objects emit electromagnetic radiation energy [3].

In non-destructive evaluation (NDE)**,** IRT is divided into two categories, as passive and active thermography [2, 3 and 4]. Passive thermography is based on the acquisition of thermography images of the object under study without external heat supply [2, 5 and 6]. In some cases, the heating is caused by the radiation from the sun, moving machinery, endothermic or exothermic process etc., [2, 5, 7]. Active thermography is based on the use of an external energy source that enables the flow of heat waves in the material [3, 5]. The energy (not always heat) source varies according to the technique employed [2, 7]. So far the techniques employed are pulsed laser and flash lamps, mechanical vibrations, induction heater, acoustic wave excitation and microwaves [5, 8]. Infrared thermography provides the following advantages.

- Fast inspection compared to magnetic particle inspection (MPI), Dye Penetration Inspection (DPI) and Visual Testing (VT) [5].
- Non-contact [5].
- Hygienic; not harmful to the environment [6].
- Results that are easy to interpret compared to MPI, DPI, and VT [6].
- Catching moving targets in real time (video rate) [9].

- Possible measurements in inaccessible and hazardous areas [9].

With the advantages mentioned above, it is of interest to find out where in the mechanical maintenance arena, IRT can be employed effectively. This study evaluates the effectiveness of IRT to enhance and alleviate the difficulty in detecting internal leaks through isolation valves. The study also explores the use and the effectiveness of infrared thermography as an alternative to the traditional NDT techniques, such as MPI, DPI and VT, and the conventional NDT technique of Ultrasound Testing (UT).

1.2 Internal Leaks

Internal leaks occur in a pipeline system due to a failure of internal barrier components such as isolation valves, steam traps, safety valves and heat exchanger tubes. These leaks cannot be observed by the naked eye; only their symptoms can be noticed, particularly when there are many such components in a system, then it becomes difficult to pinpoint the root cause of an internal leak. In principle, under normal circumstances, the high-pressure system will leak through to a low-pressure system and disturb the operation and design parameters of the system, which can lead to plant anomalies. Figure 1.1 illustrates the effects of internal leaks.

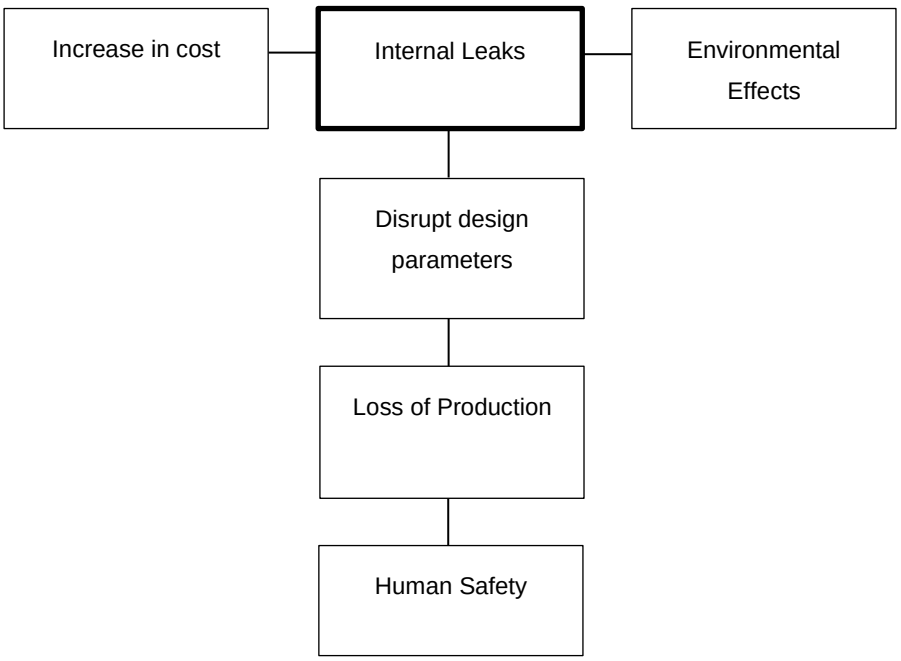

Figure 1-1. Effects of internal leaks

In a plant, the disruption of design parameters such as pressures, temperatures, and contamination from foreign substances can cause loss of production and compromise human and environmental safety. The increase in cost due to internal leaks includes expenses in detecting the internal leaks, the recovery strategies to restore the plant to its original state and maintenance of in-service components. Environmental mishaps include the contamination of natural resources such as drinking water, seawater, and soil.

The early detection of any leaks internal or external, whether it is steam, water, oil, air or gases, is very important for early decisions to be made to prevent loss of inventory in the system, which can lead to the deterioration of a system's performance, safety can be compromised and complicate its maintenance [10 and 11]. These leaks need to be detected and resolved as soon as possible. Thus a technique is required to detect internal leaks before catastrophic events occur. In this study, internal leak detection from isolation valves and safety valves will be attempted/performed using Infrared Thermography. The failure of isolation valves and safety valve to perform its desired function can lead to internal leaks, which can be highly expensive to resolve. Usually, the leak is due to the valve not being closed properly, i.e. the valve seat is not square with the plug, erosion of the seat or plug material, wear on the valve seat, valve seized etc.

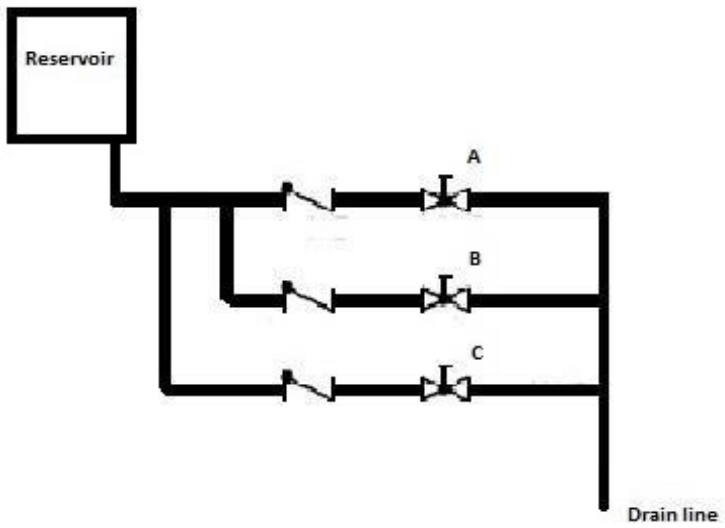

Figure 1-2. Typical schematic diagram of a Pipe network with isolation valves connected in parallel

The main concern in this study is a scenario where valves are connected in parallel pipes (as indicated in Figure 1-2) draining to a common drain header. It becomes difficult to identify which of the valves is leaking when the medium/fluid is observed at the common

drain header (drain line) [12]. In a situation like this, hours are spent trying to determine the source of the problem. In this study the use of IRT as a diagnostic inspection tool for the detection of internal leaks will be investigated. The passive thermography technique will be used to detect internal leaks through the isolation valves and safety valves, where the system's temperature is the main variable that has to be monitored.

The concern mentioned previously was observed on a drain recovery system of a power plant. Where the leak was observed on the main drain line but it could not be determined which of the valves was leaking. Figure 1-3 illustrates a typical system with valves connected in parallel, draining to a common recovery receiver. During operation, the valves are supposed to be closed therefore condensed steam is not expected on the main drain line. However, in this scenario, condensed steam was observed on the main drain line, and that is an indication of leaking valve(s). It becomes difficult to pinpoint the leaking valve and opening the drain receiver hatch poses a risk of burns to the operator/investigator.

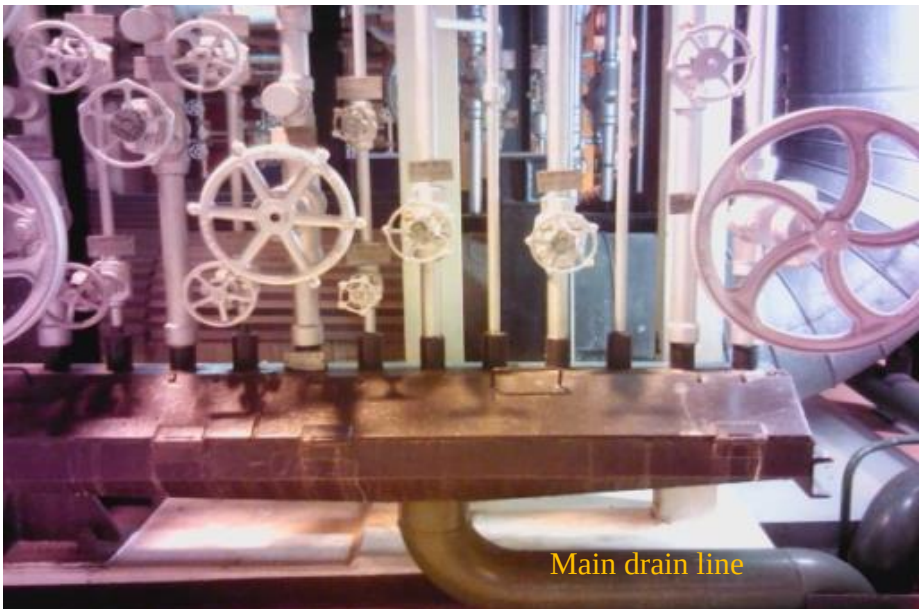

Figure 1-3. Plant configuration of parallel isolation valves

During the performance test on the main steam line of a power plant, 'leaking" steam was observed on the exhaust manifold silencer, (see schematic diagram in Figure 1-5). In this scenario, it was difficult to identify which of the safety valves were leaking when steam was observed on the manifold because they all discharged to a common manifold. Figure 1-4 illustrates the safety valves and discharge pipes to the manifold.

Figure 1-4. Plant configuration of safety valves and discharge pipes

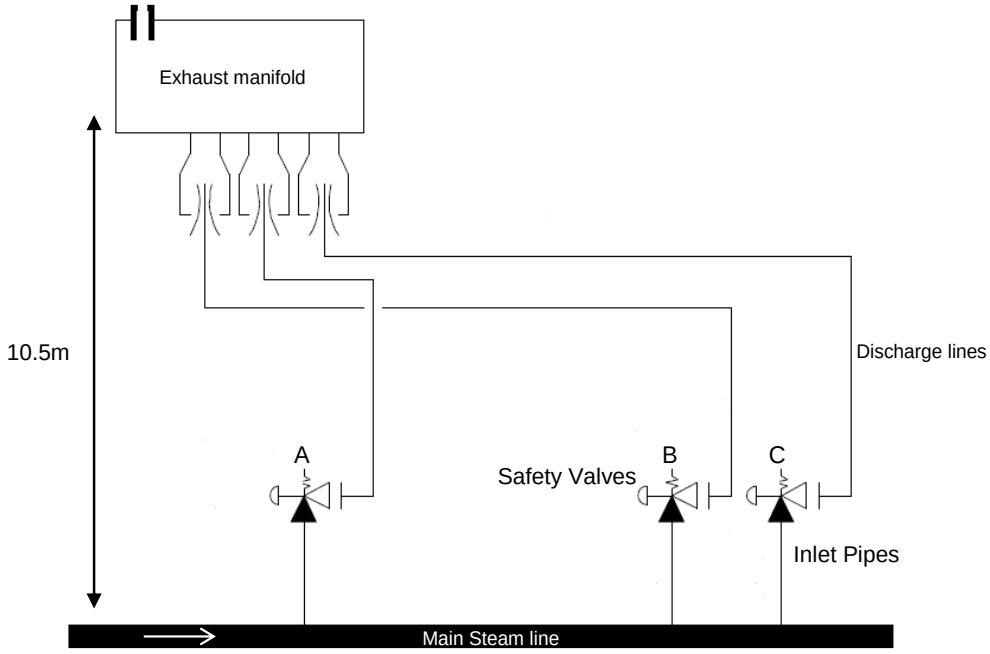

Figure 1-5. Schematic diagram of the Pressure relief system of the main steam line

The methods suitable that industries use to detect leaks through leaking process valves, steam traps, and safety valves are Ultrasound and Acoustic test. These techniques are attempted to pinpoint the leaking component [10 and 11]. The ultrasonic wave which is caused by the leaking fluid can be detected by special equipment. However, the use of such equipment is limited due to the environment (background noise) and the orientation of the valves, Acoustic testing is used when it is difficult to use IRT especially on the line that carries fluids at ambient temperature.

For both scenarios of leaking valves (as described above) a technique is required to identify the faulty one(s) without interrupting the operations of the plant, thus affecting its production and compromising human and environmental safety. As mentioned by Sulaiman [13], with IRT costs are reduced, process interruption can be planned to avoid unexpected loss of production, and harmful effects on the environment may be reduced.

1.3 Non-Destructive Evaluation of Plant's Components

The conventional NDT techniques (MPI, DPI, VT, and UT), mentioned previously are used for the inspection of surface and subsurface defects on valve stems, pipe surfaces, vessels, tanks, composite material and other mechanical equipment. These techniques are used effectively and entrusted by industries to inspect metallic components [6]. However, in this study aspects of Infrared thermography (Pulse Thermography and Induction Thermography) will be evaluated as an alternative or an additional NDT technique to the conventional ones, for the detection of defects on some of the above-mentioned plant's components. This study will compare infrared thermography with conventional NDT techniques. Induction excited thermography will be compared with MPI and DPI for the detection of surface defects, and pulse thermography will be compared with UT for the detection of subsurface defects.

Suhas [14] performed a study considering the comparison between pulse thermography and ultrasound testing on 3mm steel plates bonded structures with silicone rubber layer in between. The study considered IRT to have an advantage over UT inspection in terms of quickly detecting the defect (artificial induced delamination) between the steel plate. However, regarding the sizing of the defects IRT is not recommended to perform this operation. The results obtained from the UT testing were informatively accurate in terms of defect sizes and location, however in comparison very time-consuming in locating the defects.

Xingwang *et al* [15] used IRT and UT to detect cracks on aluminum parts. The UT technique was used as an excitation source while the infrared camera monitored the temperature profiles of the aluminum parts. The combination of the two techniques is known as

Ultrasound - excited infrared thermography. Their results indicated that the technique can effectively detect closed cracks/defects that have been previously considered undetectable by traditional NDT techniques.

Patrick *et al* [16] conducted a study determining the capability of induction stimulated infrared thermography for non-destructive testing of forged parts. The comparison was conducted between Induction Thermography and Magnetic Particle Inspection on a batch of 26 cracked wheel hubs. This study was to introduce induction thermography as an alternative NDT technique to MPI. The results indicated that Induction thermography provides better results than MPI, is a quick and environmentally friendly technique. Figure 1-6 illustrate the results obtained during wheel hub inspection.

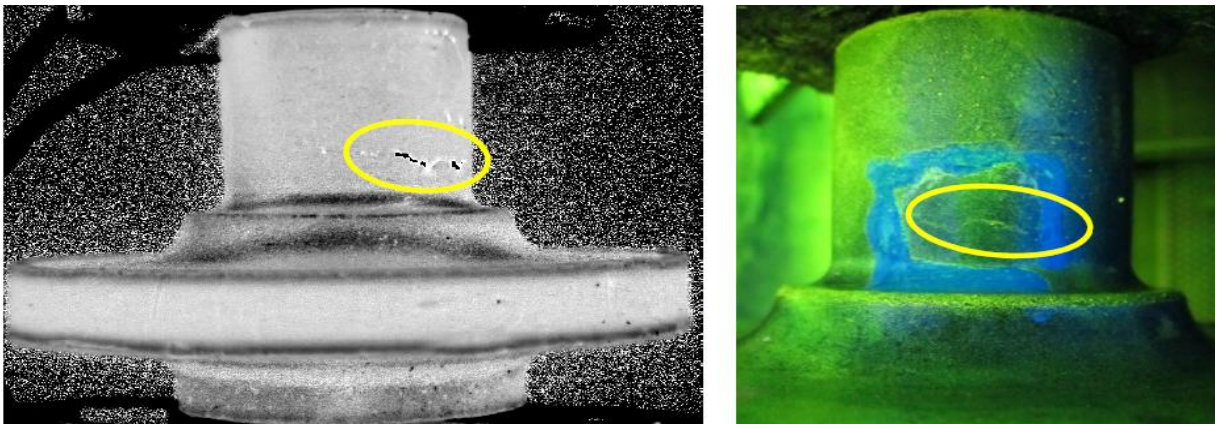

Figure 1-6. Wheel hub results, thermography results on the left, and MPI results on the right

(Adopted from Patrick *et al* [16])

Patrick *et al* [16] also compared the NDT technique of IRT using induction thermography, and the traditional dye penetration inspection, on artificial hip joint manufactured from titanium, austenitic and cobalt-based alloy. The results indicated that induction excitation IRT revealed more details of the defects compared to the dye penetration inspection. The results also revealed that induction heating IRT is well suitable for ferromagnetic material, but less efficient on titanium, stainless steel, and cobalt-based alloys because of low thermal conductivity.

1.4 Main Objectives

The main objective of this study is to investigate aspects of infrared thermography for non-destructive testing in the mechanical maintenance arena. The intention is to compare the effectiveness of detecting defects using infrared thermography with those achieved using traditional/current NDT techniques in the mechanical maintenance areas of interest in a power plant.

1.5 Organisation of the Project

This dissertation contains four chapters and four appendices. Chapter 1 is an introduction to the subject covered in this study. Chapter 2 is a literature review, where the fundamental principle of infrared thermography and the two modes of IRT active and passive thermography are presented. Chapter 3 provides the results obtained from the various experiments. It also provides the results obtained from the traditional NDT techniques of UT, MPI, and DPI. Chapter 4 is the discussion and conclusions of the results obtained.

CHAPTER 2: LITERATURE REVIEW

2.1 Infrared Thermography

Infrared Thermography (IRT) is a technique used to capture and process thermal information from equipment that radiates electromagnetic energy [2, 17]. It is a technique that processes the invisible thermal profile of any object to visible thermal images. This technique applies to all objects that have a temperature above absolute zero-degree temperature, since these objects emit electromagnetic radiation energy [3]. The electromagnetic radiation energy is directly proportional to the surface temperature and the emissivity of an object. The emissivity is defined as the ability of an object to emit infrared energy [5]. Since the energy emitted by the object is not visible to the naked eye an infrared camera is used to capture and process the thermal information to visual thermal images.

Infrared radiation (IR) energy is in the form of rays and it falls within the range of 0.75μm to 100μm (wavelength) of the electromagnetic spectrum [2, 17]. Equation 1 defines the electromagnetic energy emitted by any object and received by the camera as the product of emissivity of an object (ε_{obj}), Stefan-Boltzmann constant ($\sigma = 5.670 \times 10^{-8} W.m^{-2}.K^{-4}$) and the fourth power of the object's absolute temperature (T_{obj}), assuming no absorption loss by the medium separating the emitter and camera [2].

$$Q_{obj} = \varepsilon_{obj} \times \sigma \times \left(T_{obj}\right)^4 \tag{1}$$

From equation 1 the emissivity of the object can be calculated by finding the quotient of the energy emitted by the body to the maximum-energy that could be emitted by a 'blackbody' at the same temperature, (see Equation 2).

$$\varepsilon_{obj} = \frac{Q_{obj}}{Q_{blackbody}} \tag{2}$$

Whereas the energy emitted by the blackbody can be calculated using Planck's Law, (see Equation 3) where the power emitted is per unit area and per unit wavelength [15, 16]. C_1 and C_2 are constants, λ is the wavelength and T is body's absolute temperature.

$$Q_{\lambda b} = \frac{C_1 \lambda^{-5}}{e^{\frac{C_2}{\lambda T}} - 1} \tag{3}$$

Figure 2-1 illustrates the distribution of the electromagnetic radiation energy emitted by a blackbody at different temperatures. It shows the amount of energy emitted at each wavelength. Norman [17] stated that as the temperature increases the amount of the electromagnetic radiation emitted at each wavelength also increases.

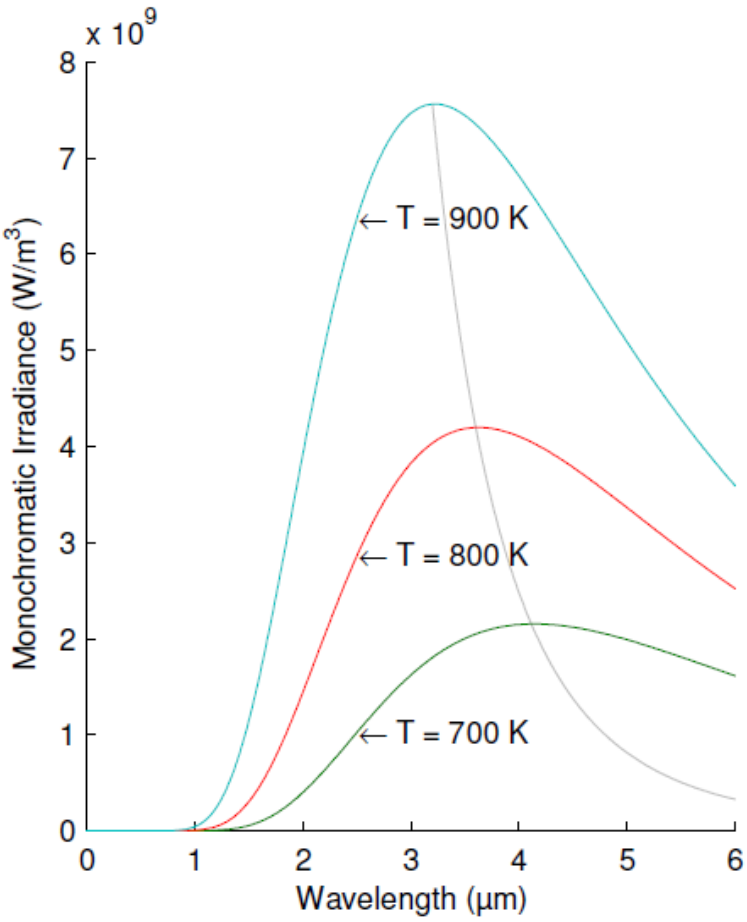

Figure 2-1. Plankian Curves for blackbody emissions at various temperatures, (Adopted from Ruben *et al* [2])

IRT being a non-contact non-destructive evaluation (NDE) method; measures the electromagnetic energy emitted from a component using an infrared camera (defined as a spectral radiometer). The camera measures the energy emitted from the component's surface and distributes it accordingly to degrees of surface temperature, which gets displayed in the form of thermal images [15, 16, and 17]. IRT is used effectively in either passive or active mode in the medical field, electrical and mechanical equipment, fluid systems, building applications, condition monitoring and in non-destructive evaluation [2, 7].

2.2 Passive Thermography

Passive thermography is based on the acquisition of images of the object under study without external heat supply, the temperature induced is natural. In some cases, the heating is caused by the radiation from the sun, moving machinery, running plant, friction, endothermic or exothermic process, fission process etc. [2, 5]. The technique is used in quality control and condition monitoring applications because temperature plays a crucial role in many industrial processes [2]. Figures 2-2 and 2-3 is a typical example of a passive thermography technique, where a running motor emits electromagnetic energy without external source applied. The energy is due to moving parts such as bearings (friction), the rotor of the motor, and electric current resistance.

Figure 2-2. An in-service pump coupled to its motor (normal image)

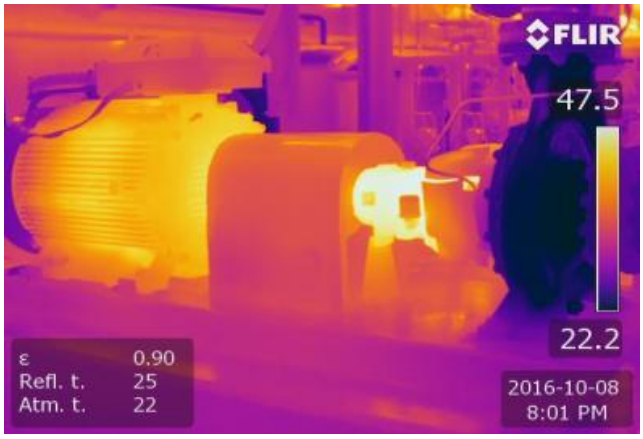

Figure 2-3. Thermal profile of the in-service pump shown in figure 2.2

2.2.1 Internal Leak Inspection Passive thermography

For this study, passive thermography will be used as a diagnostic tool to detect internal leaks through isolation and safety valves. It is expected that this technique will be successful by comparing the thermal images of the pipes upstream and downstream of a leaking valve. The change of the temperature of the pipe's surface downstream of a valve will depend on the amount of energy released by the leaking fluid, provided that the fluid's temperature exceeds the environment's level.

2.3 Active Thermography

Active thermography is based on the use of an external energy source that enables the temperature change in the material. According to Rodrigues *et al* [4], the application of active thermography to detect defects in materials began in the decade from 1960 to 1970. "That was when electronics and optics systems in the infrared band started to be employed in aerospace and nuclear engineering". However, the poor operational characteristics of infrared systems in those years caused the development of this NDT technique to be delayed. Aerospace industries use various forms of active thermography to detect, for example, the delamination of composite materials. The thermal excitation source varies according to the particular IRT technique in the following list

- Pulsed thermography
- Long pulsed thermography
- Lock-in thermography
- Induction thermography
- Mechanical vibration thermography

However, this study will consider two types of active thermography techniques; Pulse thermography and induction thermography, and give a brief discussion about other active thermography techniques.

2.3.1 Pulsed Thermography

Pulsed thermography is an active thermography non-contacting non-destructive testing (NDT) technique used to detect subsurface defects in monolithic materials and delamination in composites [2, 5 and 19]. In principle, a specified quantity of energy in the form of heat

pulse is applied to an object for a fraction of a second while using an infrared camera to monitor the temperature decay curve of the surface as the heat travels through the material [20, 21 and 22]. Figure 2-4 is a typical setup of pulse thermography.

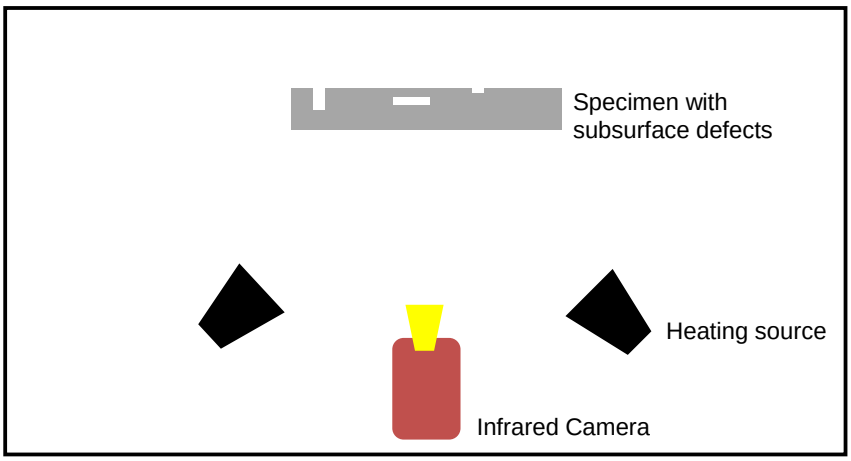

Figure 2-4. Pulse thermography set up

The heat source for pulse thermography can be flash lamps, halogen lights, heating gun, hair dryer and laser beams. It is fast in inspection and is easy to operate. The drawback of the technique is that; the non-uniform application of heat and variation of surface emissivity might affect the results [22].

According to Sheregii [23], the heat propagation through the thickness of the specimen after excitation can be explained by a one-dimension solution of the Fourier's law. The time depended on surface temperature response to heat pulsation is given by equation 4 [22, 23].

$$T(t) = T_0 + \frac{Q}{e(\pi \times t)^{1/2}} \tag{4}$$

where, Q (J) is energy absorbed by the surface of the test pieces, T_0 (^0C) is the initial temperature, t is the time (the rate of heat propagation) in seconds, e $(W.s^{1/2}.m^{-2}.K^{-1})$ is the material's effusivity which is defined by [20 and 23] as an ability of the material to exchange heat with the surrounding. Francisco *et al*, [20] mention that the effusivity of a material can be expressed by equation 5.

$$e = (k \times \rho \times c_p)^{1/2} \tag{5}$$

In equation 5, k $(Wm^{-1}K^{-1})$ is the thermal conductivity of the material, ρ $(kg.m^{-3})$ is the density and c_p $(Jkg^{-1}K^{-1})$ is its specific heat [13].

According to Almond *et al* [24], equation 5 could be modified to equation 6 specifically to simulate thermal response(contrast) of materials with circular subsurface defects.

$$T_C(t) = \frac{2Q_0}{\sqrt{\pi \rho c_p kt}} \left(\sum_{n=1}^{\infty} e^{-\frac{(nd)^2}{\alpha t}} \right) \times \left(1 - e^{-\frac{\left(D/2\right)^2}{4\alpha t}} \right) \tag{6}$$

where Q_0 (J) is the initial heat energy applied on the surface of the specimen, d (mm) is the depth of the defect, D (mm) is the size of the defect, t is the response time in second and α ($m^2.s^{-1}$) is the thermal diffusivity that measures the material's ability to conduct heat in relation to its capacity to store it [20 and 23]. Thermal diffusivity is defined as an indicator that can be used to check how quickly a material will change the temperature in response to the application of heat Wrobel at al [25]. Thermal diffusion is a thermo-physical property that is directly proportional to thermal conductivity and inversely proportional to material density and specific heat (see Equation 7).

$$\alpha = \frac{k}{\rho \times c_p} \tag{7}$$

According to Grzegorz [26], hot spots in areas over flat bottom holes (FBH) (subsurface defect) are observed as an indication of a high concentration of heat trapped between the surface and subsurface defect (see Figure 2-5).

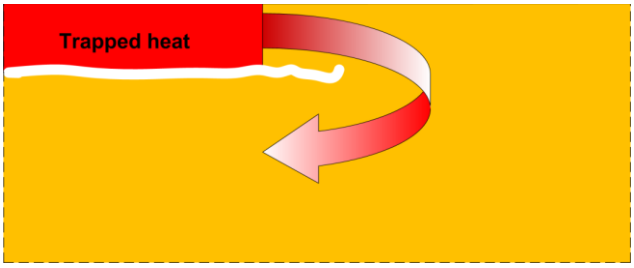

Figure 2-5. Trapped heat flows around the defect
(Adopted from Grzegorz Stanislaw Ptaszek [26])

2.3.2 Long Pulse Thermography

Long Pulse Thermography also known as Square Pulse Thermography which is defined as Pulse Thermography with relative long heating excitation period, typically at least a couple of seconds of heating compared to the traditional Pulse Thermography [19 and 30]. The

technique was introduced to extend the Pulse Thermography analysis of results. Long Pulsed Thermography is suitable for materials that required long pulsation such as buildings, plastics and thick composites [19]. It can also be used to detect subsurface defects such as cracks, delamination, impact damage and moisture ingress or content in the aerospace and aircraft industries [30]. Generally, the technique can be processed to improve defect visibility and perform qualitative studies of defects.

2.3.3 Induction Thermography

Induction Thermography has been in use since the 1970's to test steel bars in roll mills for cracks [27]. The fundamental concept of this method is that an alternating current is induced in an electrically conducting material by a charged coil or electric wire placed near the inspection surface. An induced current will flow in the opposite direction to the coil and wire current. Any crack on the specimen will disturb the induced current flow and cause it to flow around the crack [27 and 28]. Thus heat will be generated due to a high concentration of current density on the crack tip, (see Figure 2-6).

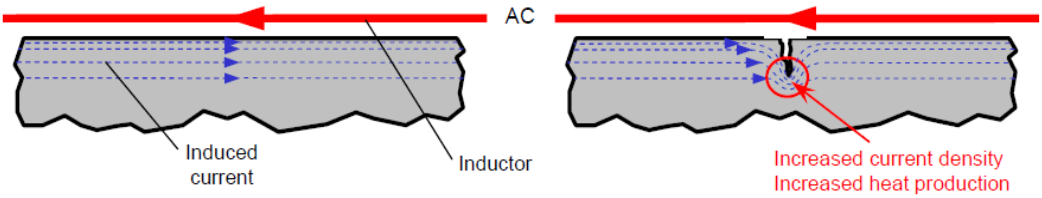

Figure 2-6. Induction heating Thermography principle
(Adopted from Vrana *et al* [27])

The induced current in a specimen flows to a certain depth from the surface; this is governed by the well-known skin effect. Vrana *et al* [27], say it depends on the frequency of excitation, electric conductivity and magnetic permeability of the material. Figure 2-7 shows the relationship between frequency and skin depth measured on a 304L stainless steel specimen. As stipulated by the graph and equation 8, the penetration depth increases as the frequency reduces.

$$\delta = \frac{1}{\sqrt{\pi \cdot \mu \cdot \sigma \cdot f}} \tag{8}$$

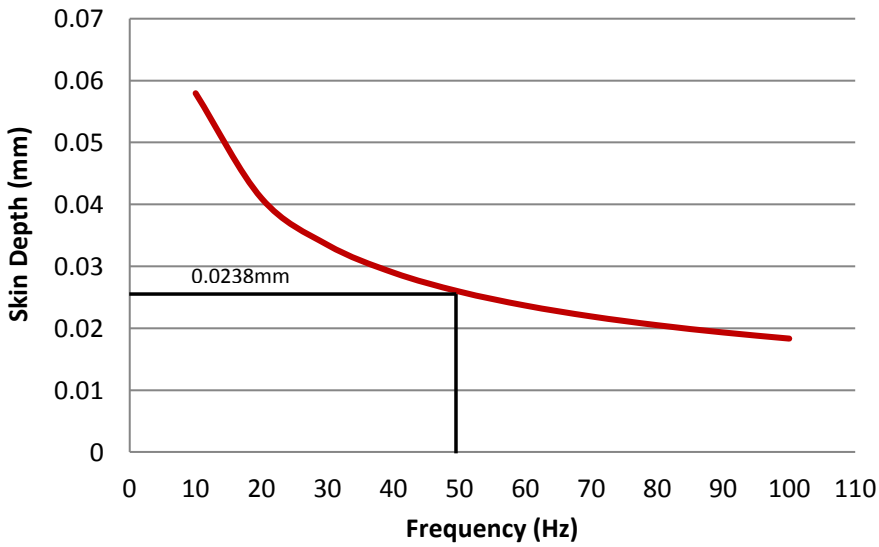

Figure 2-7. Penetration depth vs Frequency for 304L Stainless steel

The penetration depth of the induced current, $\delta(m)$ is given by equation 1, f is an excitation frequency (Hz), σ is the electrical conductivity (S/m), and μ is the permeability (Hz/m) of the material. When the excitation frequency induced in 304L stainless steel is 50Hz the theoretical penetration depth will be $0.00238mm$.

The material under test gets heated by its resistance to the induced current flow. The heat generated is inversely proportional to the electric conductivity and proportional to the square of the magnitude of the electric current's density [29]. The heat emitted (hot-sport) by the test piece can be formulated as shown by equation 9.

$$Q = \frac{1}{\sigma}|J_s|^2 = \frac{1}{\sigma}|\sigma E|^2 \qquad (9)$$

Where σ the electric conductivity is (S/m), J_s is the current density (A/m^2) or electric field intensity E (N/C). As mentioned previously, the presence of any defect in a material will restrict the induced flow which can result in a localized high current density and hence a localized increased heat generation. The localized heat generated will affect the surface's thermal profile which is being monitored by the infrared camera.

2.3.4 Lock-in Thermography

In Lock-in Thermography the surface of the specimen is periodically illuminated by sine modulated energy which is converted to sine modulated heat [21 and 22]. The periodic wave propagates by radiation through the air to the surface of the specimen, where heat is produced and propagate through the material by conduction. In some cases, halogen lamps

are used as an exciting source to inject thermal waves into the specimen [5 and 22]. Figure 2-8 illustrates a typical setup of lock-in thermography. This technique is recommended for the detection of subsurface defects. It gives good information about defect size, depth and thermal resistance [21]. During excitation, the defects inside the specimen act as a barrier and prevent thermal waves from propagating homogeneously. Larbi *et al* [22], states that the defects cause a change in amplitude and phase delay to the response signal returning to the surface, then an Infrared camera is used to record the temperature change on the surface of the specimen. Figure illustrate the Lock-in thermography set-up.

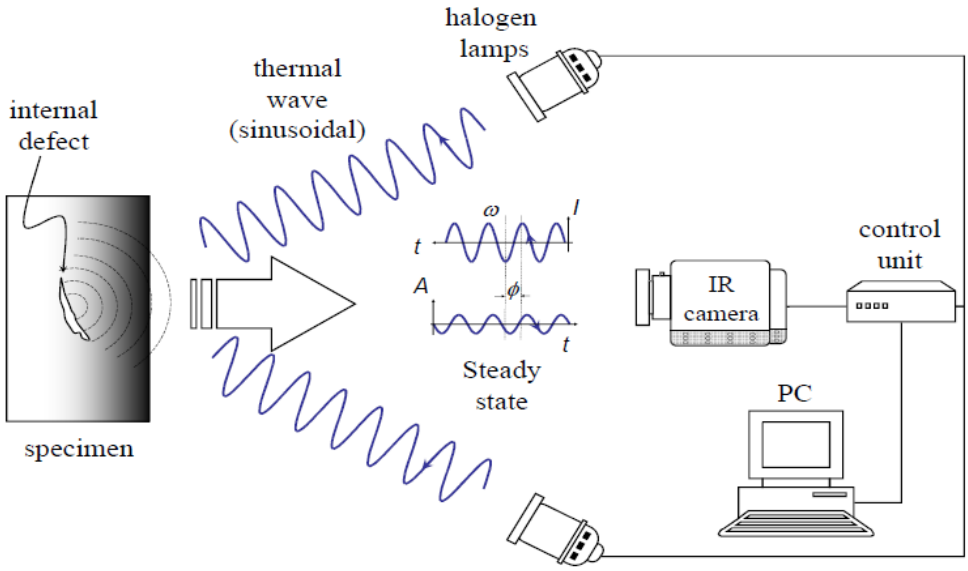

Figure 2-8. Typical setup for lock-in thermography
(Adopted from Larbi *et al* [22])

According to Larbi *et al* [22], Fourier's analysis is the preferred processing technique to extract the amplitude and phase information of the surface of the material since it provides single image, ampligrams / phasegrams. Equation 10 demonstrate the Fourier's law one dimensional solution for a periodic thermal wave propagating through a semi-infinite homogeneous material.

$$T(z,t) = T_0 \exp\left(-\frac{z}{\mu}\right)\cos\left(\frac{2\pi z}{\lambda} - \omega t\right) \qquad 10$$

where $T_0\,(^0C)$ is the initial temperature produced by heat source, $z\,(m)$ $\omega\,(rad/s)$ is the modulation frequency which can be expressed as ($\omega = 2\pi f$, with f being a frequency in Hz), $\lambda\,(m)$ is the wavelength, and $\mu\,(m)$ is diffusion length given by ($\mu = \sqrt{2\alpha/\omega}$). The

increase in frequency will improve the Lock in Thermography in revealing the subsurface defects, however, the maximum depth of a defect is limited by the equipment's range of selectable frequencies. According to Ruben *et al* [2] and Xavier [5], the solution to this problem is Ultrasound Lock-In Thermography by selectively stimulating defective areas with acoustic waves.

2.3.5 Ultrasound Thermography

Ultrasound thermography also known as vibrothermography is a mechanical excitation active thermography technique that is used to detect closed crack in metals and ceramic as well as delamination and disbands in composites material [5, 15]. This technique has been proven to be a promising NDT tool for the detection of defects. Below is the typical set up of Ultrasound Thermography.

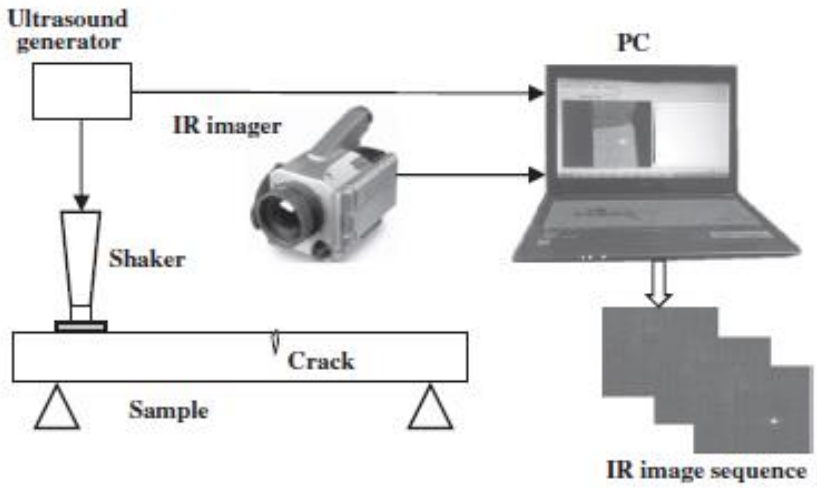

Figure 2-9 Ultrasound Thermography set-up

(Adopted from Xingwang et al [15])

In principle, the mechanical vibrations with frequency ranging from $5-10kHz$ induced by an ultrasonic generator in a specimen travel through the test piece homogenously causing the specimen to vibrate in unison. Where there is a crack or delamination, the two defect faces will not move in unison. Then the friction movement between the two faces will convert vibration energy to thermal energy [5]. The heat generated between the two surfaces will propagate by conduction through the material to the outer surface. An infrared camera is used to monitor the change in the temperature of the surface. The detection of the defect is influenced by increasing or decreasing the mechanical excitation frequency.

2.3.6 Post Processing Methods

According to Ruben *el at* [2], with active thermography techniques, some defects are small and cannot be observed easily, thus the signal levels associated with them can be lost in the thermographic data noise. Therefore, in such a case different post-processing methods can be used to improve the signal-to-noise (SNR) content of the thermographic data. Post processing methods include statistic moment, principle components analysis, dynamic thermal tomography, polynomial fit and derivatives [2].

The aspect of characterising the defects that have been detected, has been the incentive of rigorous research in recent past, which resulted in specific techniques of thermal excitation, and the recording of the resulting time dependent thermal contrasts, the phase shift created by the modulated heating frequency etc. The nature of these technique requires expensive equipment and lengthy computation processes. Even though the review of these techniques assisted in concluding that considerable progress has been achieved both in terms of detectability and characterization of the defects, however there are still disadvantages in terms of accuracy, process time and expense. Thus for the purpose of this study post processing methods will not be employed. Images will be modified/enhanced by using Microsoft Format Picture.

2.4 Conventional NDT Techniques

There are established long standing, known as conventional, non-destructive testing techniques that are commonly used by industries to inspect for surface and subsurface defects in metallic materials [6]. These techniques are used to inspect high-pressure and high-temperature processing pipes, pressure vessels, rotating shafts, valve stems, gears and other mechanical components [6, 31]. The methodologies of the techniques are not the same, each technique is unique [31]. The application varies depending on the surface to be inspected, the type of material and location. The following section describes the conventional NDT techniques commonly used in industry with details of particular application, function, advantages and disadvantages.

2.4.1 Magnetic Particle Inspection

Magnetic particle inspection (MPI) is a contacting non-destructive technique that is used to inspect the ferromagnetic material. This technique is capable of detecting defects open from the surface and just below the surface [32 and 33]. According to Luk *et al* [33], MPI is a combination of two NDT techniques: magnetic flux leakage testing and visual inspection.

The fundamental principle of MPI is as follows; the test piece is magnetized by using a permanent or an electromagnet through the surface of the specimen. The magnetic field induced to the specimen is composed of magnetic force lines flowing from South to the North Pole. Any surface defect on the material will disturb the flow of magnetic lines and caused the lines to exit and re-enter the specimen The exit and re-entry of the magnetic force cause the crack edges to become magnetic poles North and South which have the power to attract finely particles of iron fillings. The collection of iron fillings around the defect is an indication of the presence of a defect [33 and 34]. Figure 2-9 illustrates the working principle of MPI.

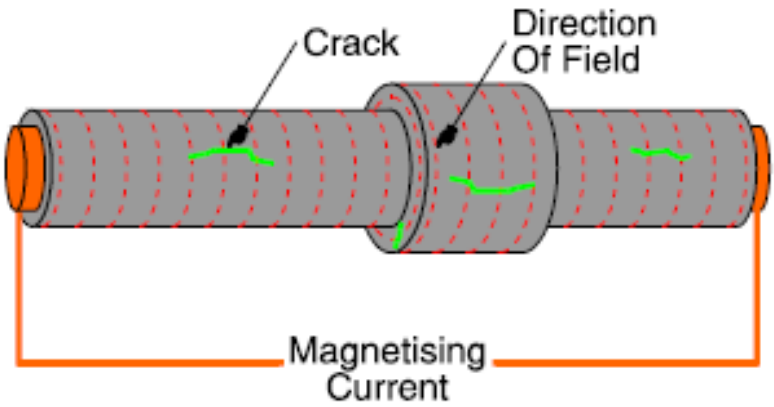

Figure 2-10. Demonstration of MPI during inspection
(Adopted from Willcox *et al* 34)

Advantages of Magnetic Particle Inspection

- Simple to operate
- The technique is not expensive
- It is rapid/quick to perform
- It is a portable NDT method
- Will work through thin coating or paint on the surface

Disadvantages of Magnetic Particle Inspection

- The piece to be tested must be of ferromagnetic materials
- Limited to the surface and near surface defects.
- The magnetic force line must be at a right angle (perpendicular) to the defect.
- Demagnetization following inspection is necessary.
- Inspection of large surfaces requires high current.

2.4.2 Dye Penetration Inspection

Dye penetration inspection (DPI) also known as liquid penetrant inspection (LPI) is a non-destructive technique that is used to inspect surface defects using colour dye [32, 34 and 35]. According to Sharon *et al* [36], the test was developed in 1940's to detect flaws on the surface of the material. The technique is very effective in detecting defects that are open to the surface. It can be used successfully on nonporous and smooth surfaces such as metals, glass, plastic and ceramics [35]. It is widely used to inspect manufactured products, castings, forgings and welded parts. Figure 2-10 illustrate a typical DPI results indicating an existing of a defect close to the weld.

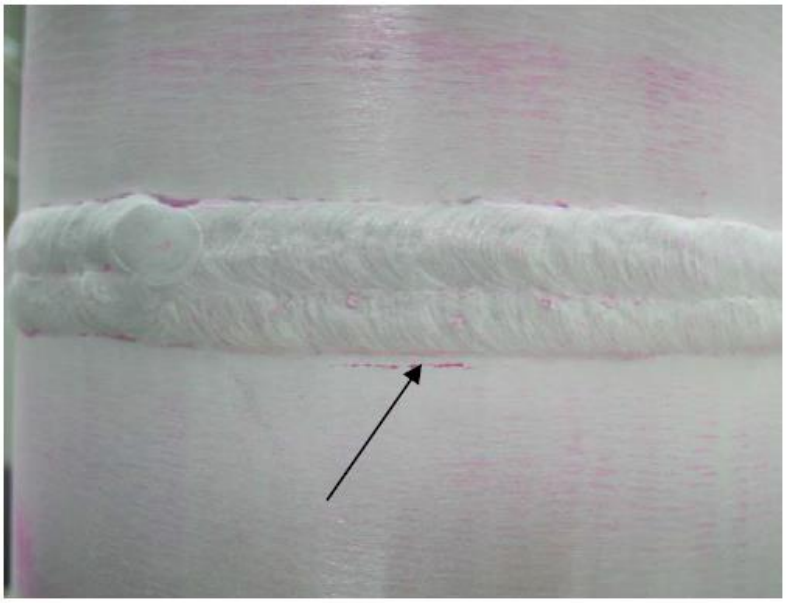

Figure 2-11. Indication of defect using DPI
(Adopted from Luk *et al* 33)

In principle, a liquid is applied to the surface to be inspected for a period of time. The time is to allow the penetrant to find access through the cracks/defects. After sufficient time has elapsed the excess penetrant on the surface of the specimen is cleaned and dried and a developer is applied to the surface being inspected. The remnants of the penetrant inside the defects are absorbed by the developer which changes colour locally. This will be the indication of an existing defect [33, 34, 35 and 36].

Advantages of Dye Penetration Inspection

- It is a low-cost technique
- It is simple to perform
- The equipment is portable

Disadvantages of Dye Penetration Inspection

- DPI is limited to surface defects
- The technique is messy
- It uses a considerable amount of consumables.
- Is limited by space and orientation of an object.

2.4.3 Ultrasound Testing

Ultrasound testing is a contacting non-destructive technique that is used to detect surface and subsurface defects and characterize the material. This technique makes use of the propagation and reflection of high-frequency ultrasound waves [34, 38 and 39]. It is usually used on steels, PVC and other metals, but it can also be used on concrete, wood, and composites.

According to Willcox *et al* [34], the UT principle is the same as that of echo sounding. An electric charge is applied to a piezo electric crystal to vibrate for a very short period at a frequency related to the thickness of the crystal (generating a short pulse of ultrasound) [38, 40]. The induced Ultrasound waves propagate homogeneously through the material. Where there is a discontinuity of material the propagation of waves will be disturbed and not

continue further and reverse with the same magnitude to the inducer [40, 41 and 42]. Figure 2-11 is an illustration of ultrasound induced and reversed due to the material discontinuity.

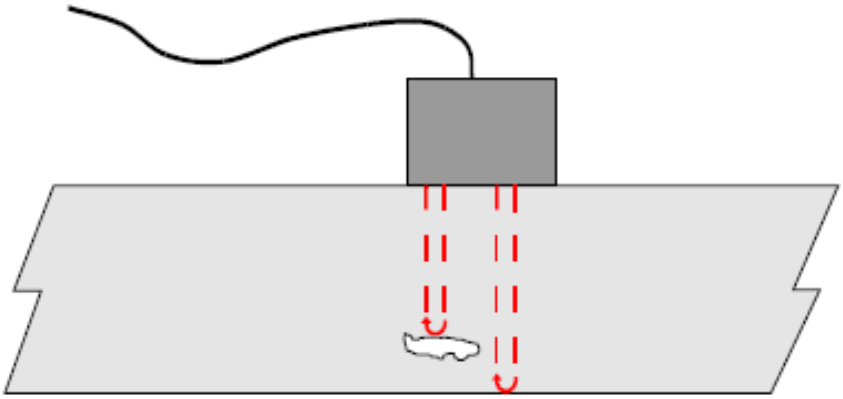

Figure 2-12. Ultrasound testing principle
(Adopted from Willcox *et al* [34])

Advantages of Ultrasound Testing

- The Technique is portable.
- No harmful consumables are used.
- The results are obtained in real time.
- Can detect defects at different positions, size, and type.

Disadvantages of Ultrasound Testing

- Requires a special skill/training and experience to obtain adequate results.
- Indications require interpretation.
- It is difficult to detect and size defects in thin material.

CHAPTER 3: EXPERIMENTAL METHODOLOGY

3.1 Introduction

This section presents the methodology that was used to investigate the effectiveness of infrared thermography (IRT) as a non-contacting non-destructive testing (NDT) technique in the mechanical maintenance arena. Three experimental methods were used to assess the effectiveness of IRT. In the first set of experiments, IRT was employed as a diagnostic technique to detect internal leaks through isolation. In the second lot of experiments, IRT was employed to detect subsurface defects in various materials, and the effectiveness was measured by comparing the methodology with the conventional NDT technique of ultrasound testing. The third set of IRT experiments aimed at detecting surface defects on metals and the effectiveness was compared with the classical NDT techniques of magnetic particle inspection (MPI) and dye penetrant inspections (DPI).

A FLIR T640 Infrared camera was used for the acquisition of data during all experiments (internal leak inspection, surface and subsurface defects' detection). Figure 3-1 depicts an image of the camera used, and Table 5-1 in appendix A-1 contains the specifications of the camera.

Figure 3-1. FLIR T640 Infrared Camera

3.2 Internal Leak Detection Methodology

The approach to validate the assumption that an inspection for internal leaks from isolation valves could be performed using an infrared camera was conducted by performing a laboratory experiment using a model fluid handling system (see Figure 3-3). The fluid handling system model was intended to obtain and prove the working principle of the technique before it was used in the plant. Figure 3-2 demonstrates schematically the infrared thermography inspection set up for the detection of leaks from isolation valves. The schematic consisting of a thermal camera, medium flowing through the system's processing pipe and an isolation valve. A and B are points used to check the change in temperature of the pipes.

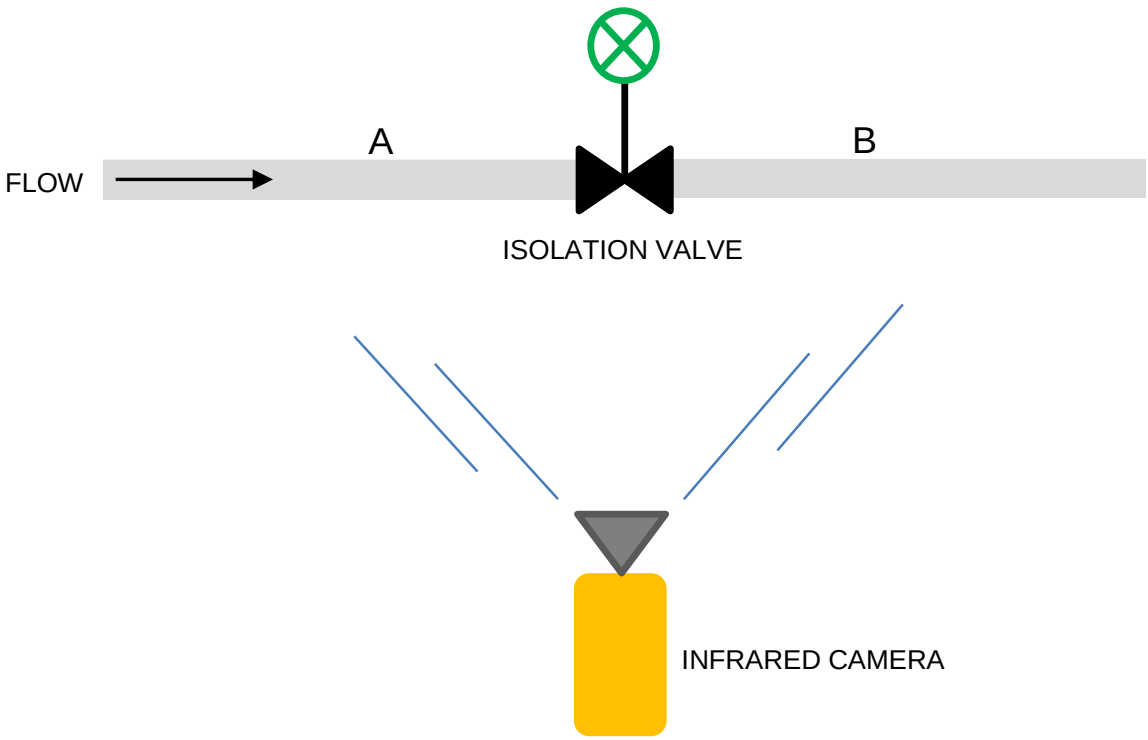

Figure 3-2. Set up of internal leak inspection using IRT

For this study, the medium flowing through the system was hot water with a temperature that was above atmospheric levels. The energy from the water was transferred by conduction through the wall thickness of the pipe raising the outer surface temperature of the pipe to above atmospheric level. The experiment performed in the laboratory used boiled water while in the plant related inspections, condensed steam flowed in the various plant systems.

The model's fluid handling system was constructed with a schedule 40 diameter of $12.7mm$ galvanized pipe. Appendix B-1 provide the sizes of the system and Table 5-2 contains the list of materials used to construct the model. A thread seal tape was used when assembling the model's pipe network to ensure no leaks when under pressure. The system was pressure tested up to $500kPa$ for leak tightness.

The Model's fluid handling system contained three $12.7mm$ stainless steel ball valves connected in parallel. The valves were connected between the pipes leaving three threads on the pipe protruded outside not to damage the Teflon seal inside the valve.

3.2.1 Experimental Procedure with the Model

Figure 3-3 illustrates the fluid handling system of the model which was secured on a wooden plinth, inclined 15^0 to the horizontal. The isolation valves were placed in closed position and the system was filled with hot water (at a temperature of $\pm 80^0$ achieved using a domestic kettle). Approximately 2 minutes' post filling the system, an infrared camera was used to measure the temperature difference across the valves.

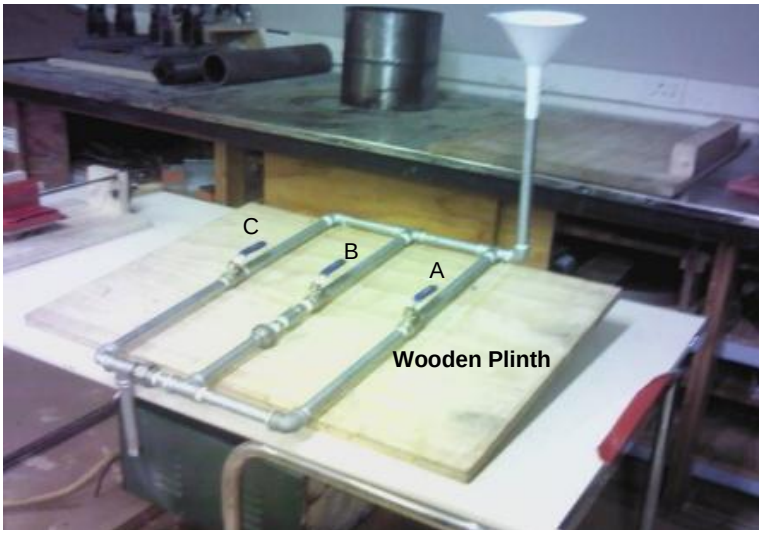

Figure 3-3. Fluid handling system mounted on wooden plinth

Thereafter maintenance valve (A) was cracked open (simulating a leaking valve) while valves B and C were maintained in their closed position (see Figure 3-4). Valve A was set slightly open such that the minimum amount of water passing through was approximately $12ml/\min$ observed in the common drain.

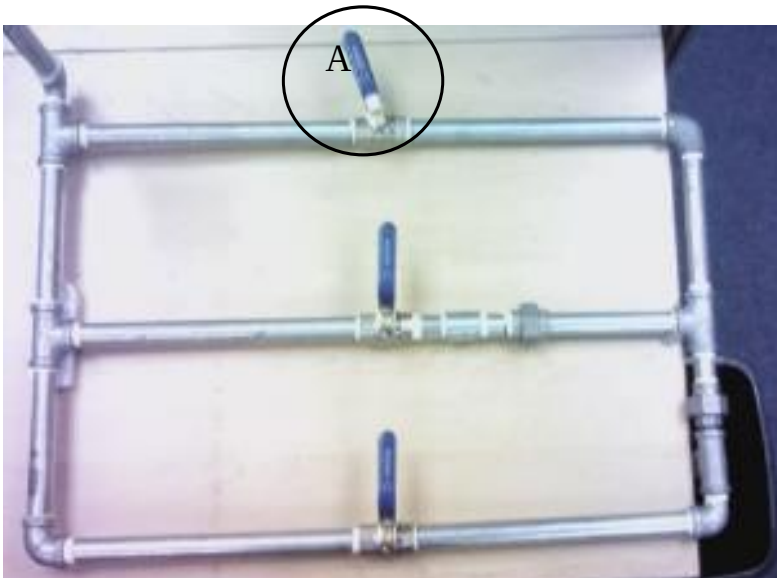

Figure 3-4. Fluid handling model with valve A cracked open

3.2.2 Laboratory (Model's) Experimental Results

Figure 3-5 is a thermal image of the system before the commencement of the experiment while Figure 3-6 demonstrates the system filled with hot water without any internal leaks noted across the valves. Figure 3-7 illustrates the system with a leak (as expected), observed by a change in the temperature of the pipe downstream of valve A. The results also indicate that valve B and C are not leaking.

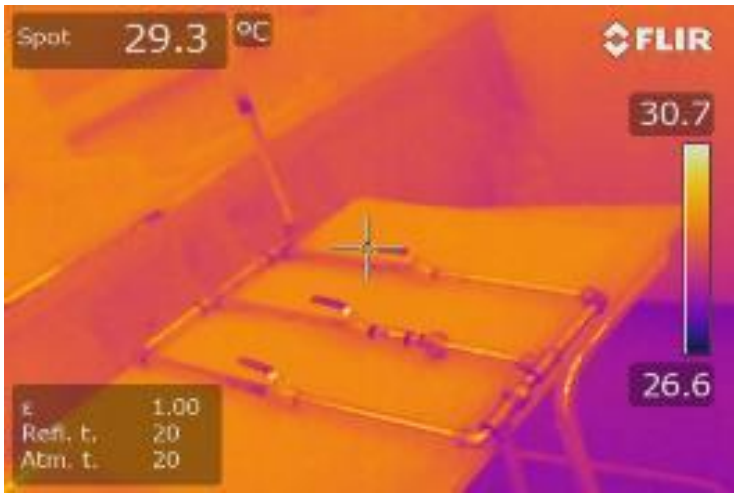

Figure 3-5. Thermal image of model's pipe network before experiment

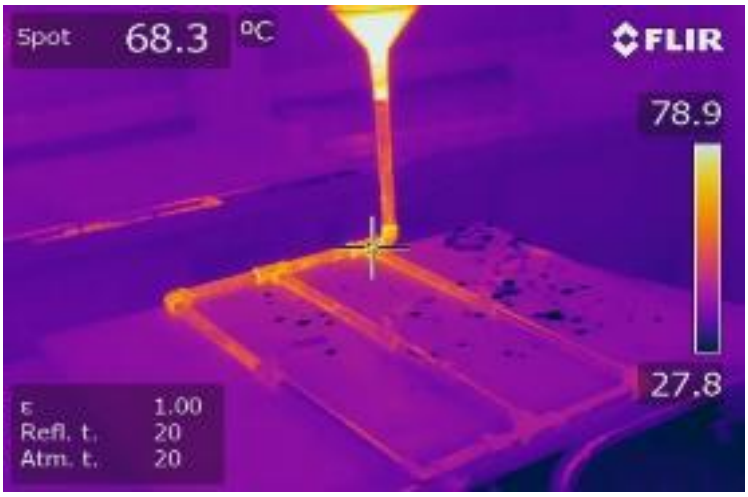

Figure 3-6. Demonstration of system without internal leaks

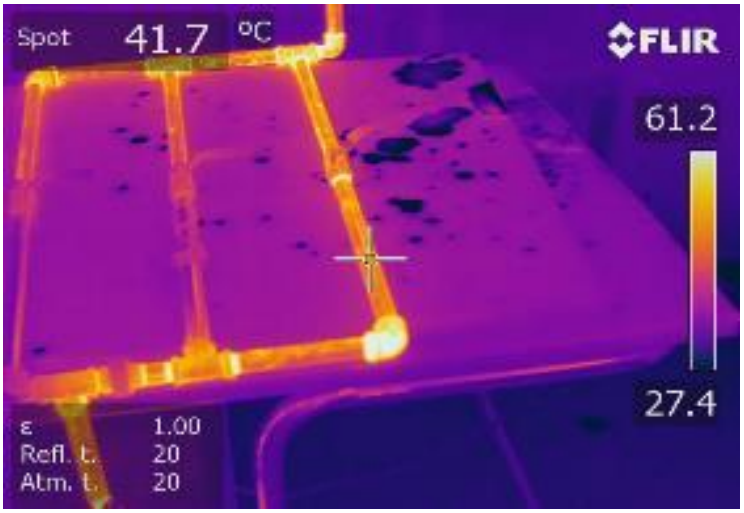

Figure 3-7. Demonstration of internal leak through valve A

3.2.3 Leak detection across Isolation Valves in the Power Plant

Three different drain systems in the power plant were identified to have potential internal leaks across their isolation valves. The drain systems in the power plant consisted of different types of valves welded between the drain pipes from different systems. Figure 1-3 is a typical arrangement of drain system with ball valves, globe valves and gate valves painted grey in colour. Other systems had double isolation valves with similar valves connected in series. The sizes of drain pipes ranged from $12.7mm$ to $63.5mm$ schedule 40. The pipes were joined together by weld and coated with grey colour paint.

The experiment was performed during plant operation and the valves were in closed position. The systems were classified as drain system A, B and C and they were assessed to have sufficient thermal energy emitted by the surface of the pipes. The emissivity of the target was measured and the camera was set to the desired emissivity. This was to eliminate other systems around the area with high thermal energy compared to the target, (see the procedure to calculate the emissivity in Appendix C-1).

3.2.4 Results of Internal Leaks through Isolation Valves

Figure 3-8 is an illustration of drain system without internal leaks. Figure 3-9 to 3-11 represent different drain systems with an internal leak.

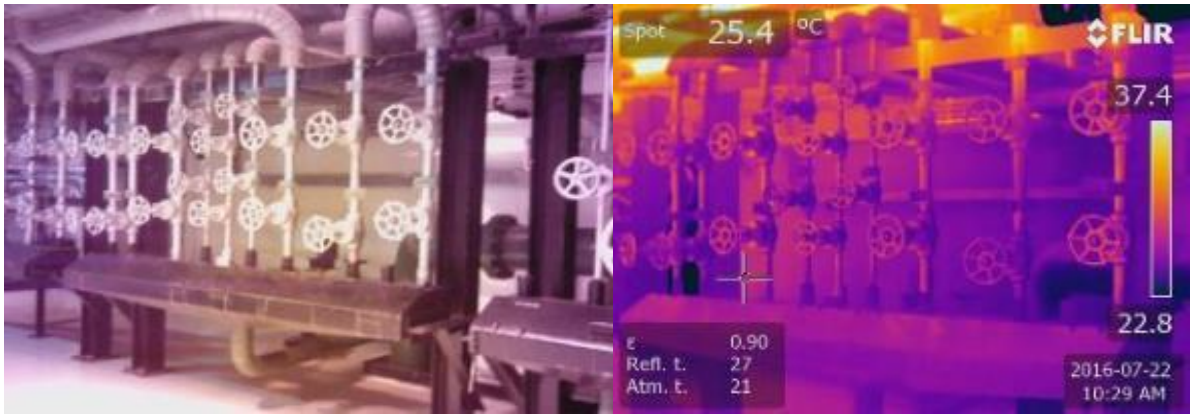

Figure 3-8. Drain system without internal leaks

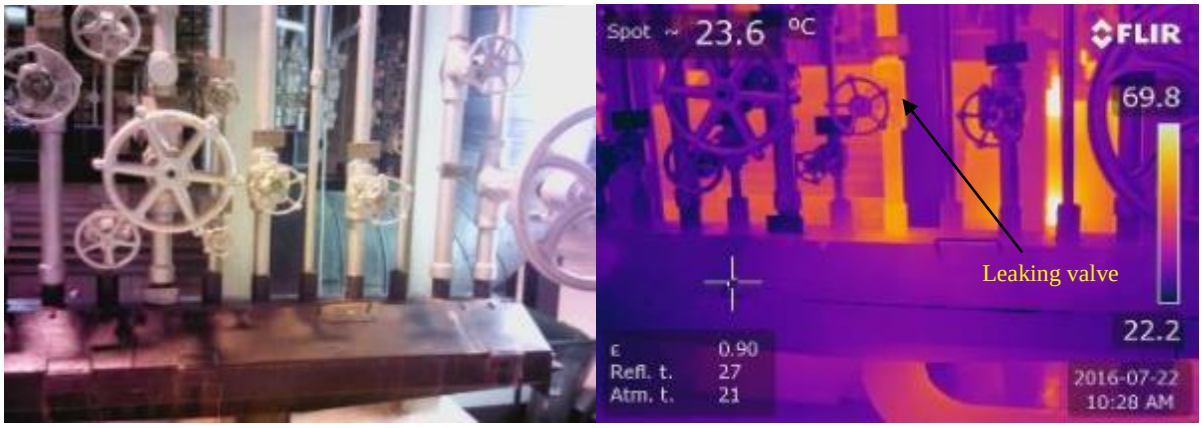

Figure 3-9. Drain system A with internal leak

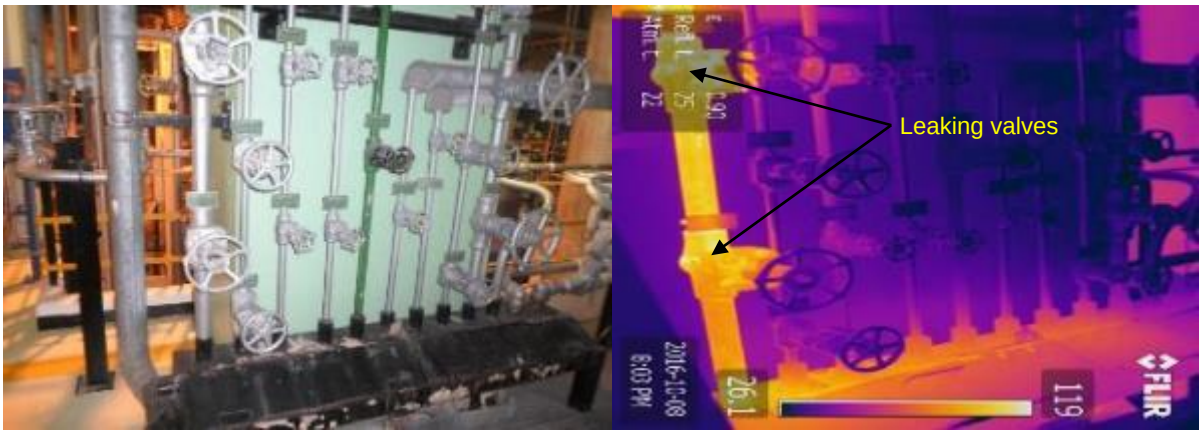

Figure 3-10. Drain system B with double isolation leaking

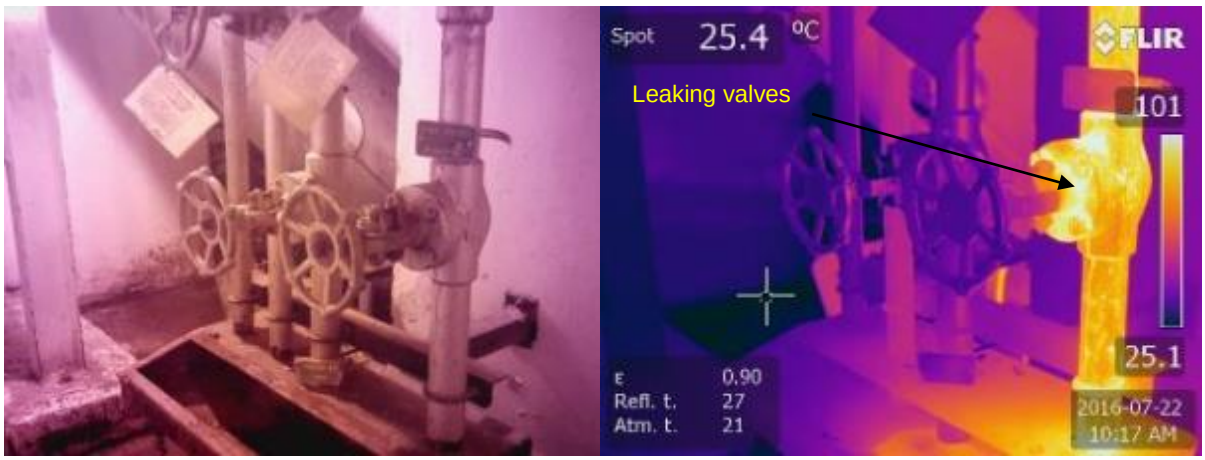

Figure 3-11. Drain system B with internal leak

3.2.5 Leak detection across Safety Valves

Three safety valves in the power plant were suspected to have potential internal leaks across their seats. These valves installed in the main steam line (180^0C of steam flowing through) of the power plant discharge to a common exhaust manifold. The leak was observed on the exhaust manifold but could not identify leaking valve(s) (see the arrangement of the valves in Figure 1-4 and 1-5). Each valve consisted of $400mm$ diameter discharge pipe.

IRT was used to monitor the temperature difference across the discharge pipes of the safety valves. The discharge pipes were classified as A, B and C. The emissivity of the target was measured and the camera was set to the desired emissivity. This was to eliminate undue

influence from other systems around the area with high thermal energy compared to the target.

3.2.6 Results of Internal Leaks through Safety Valves

Figures 3-12, 3-13 and 3-14 demonstrate the results obtained during leak detection across safety valves. The results indicate that discharge pipes A and B are likely to have fluid (steam) passing through them when compared to C, and B seems to be worse than A.

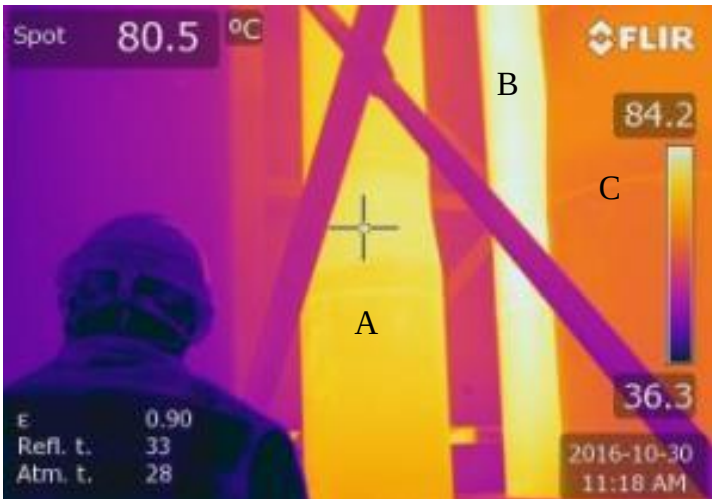

Figure 3-12. Discharge pipe A results

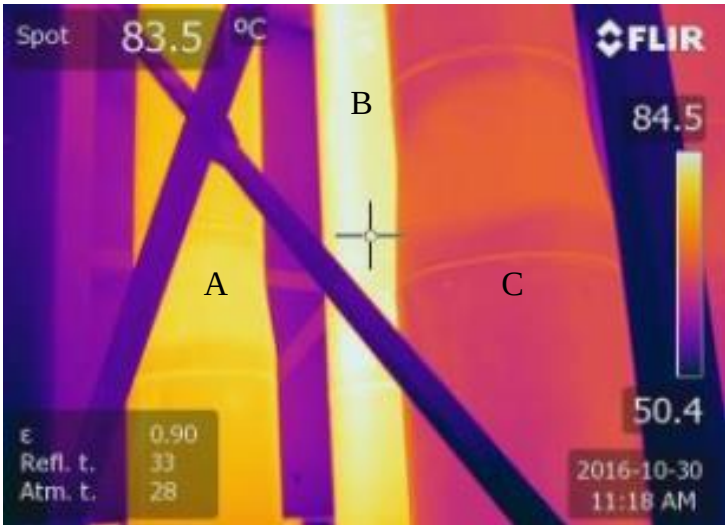

Figure 3-13. Discharge pipe B results

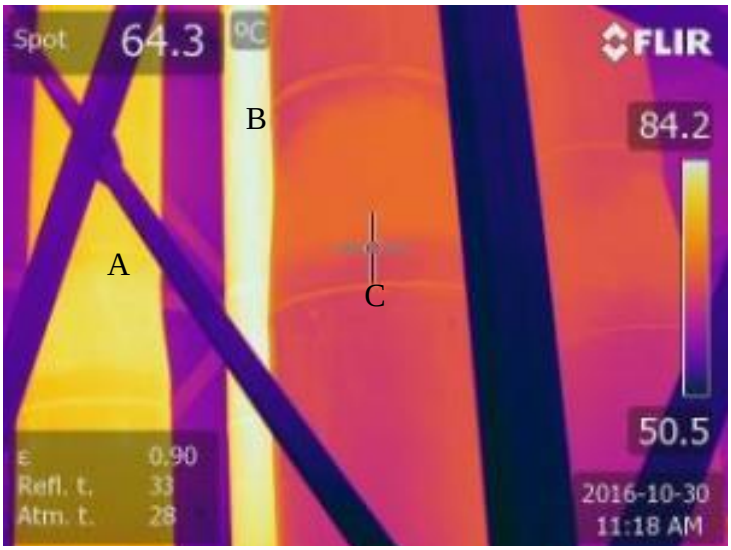

Figure 3-14. Discharge pipe C results

3.3 Pulse Thermography

The aim of this study was to assess the effectiveness of pulse thermography in detecting subsurface defects. The assessment was performed by comparing the results of this technique with the conventional NDT of ultrasound testing. Both techniques were employed to detect subsurface defects on various specimens as described below. Figure 3-15 is a typical pulse thermography set up comprising of, a heating source, the target specimen and an infrared camera.

A heating gun was used as a source to thermally excite the test specimens. the gun can produce a maximum power of $2000W$ and discharges a stream of hot air with a temperature range between $60^0C - 500^0C$. Three specimens manufactured from PVC, stainless steel, and mild steel material respectively of identical geometry (see Figure 3-16) were fabricated with flat bottom holes (FBH), of various sizes and depths, at the far side of each specimen. The near surface (surface without holes) of each specimen was coated with matt black paint to ensure uniform emissivity. A thermal camera was used to monitor the surface temperature of each specimen while cooling after having been excited by the hot air from the heating gun. During the experiment, the camera was set to video mode to capture the variation of the temperature on the surface of the specimens.

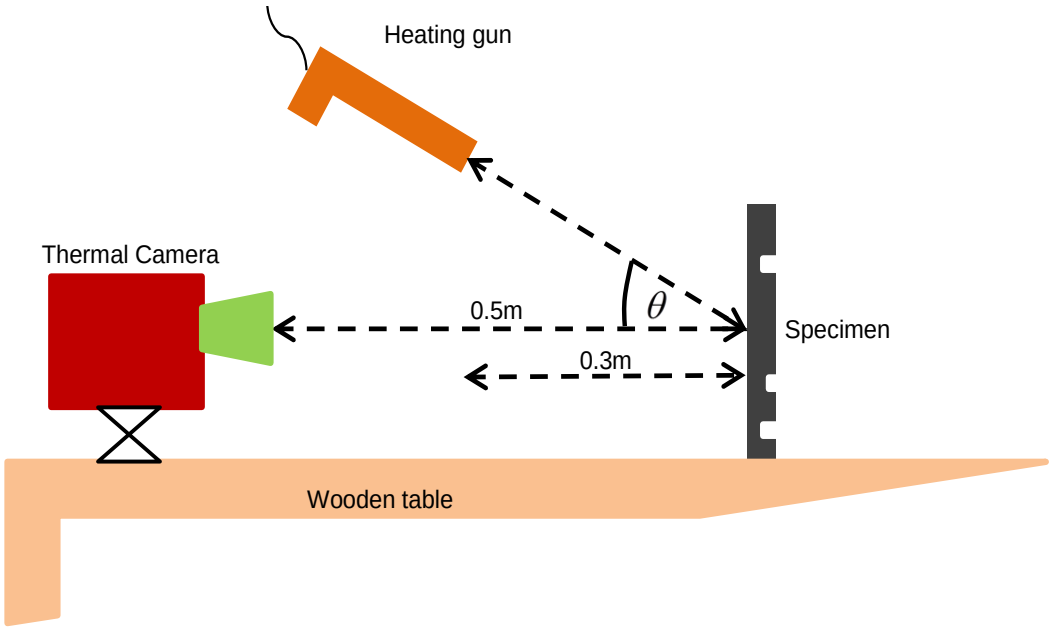

Figure 3-15. Schematic of the experimental setup of pulse thermography

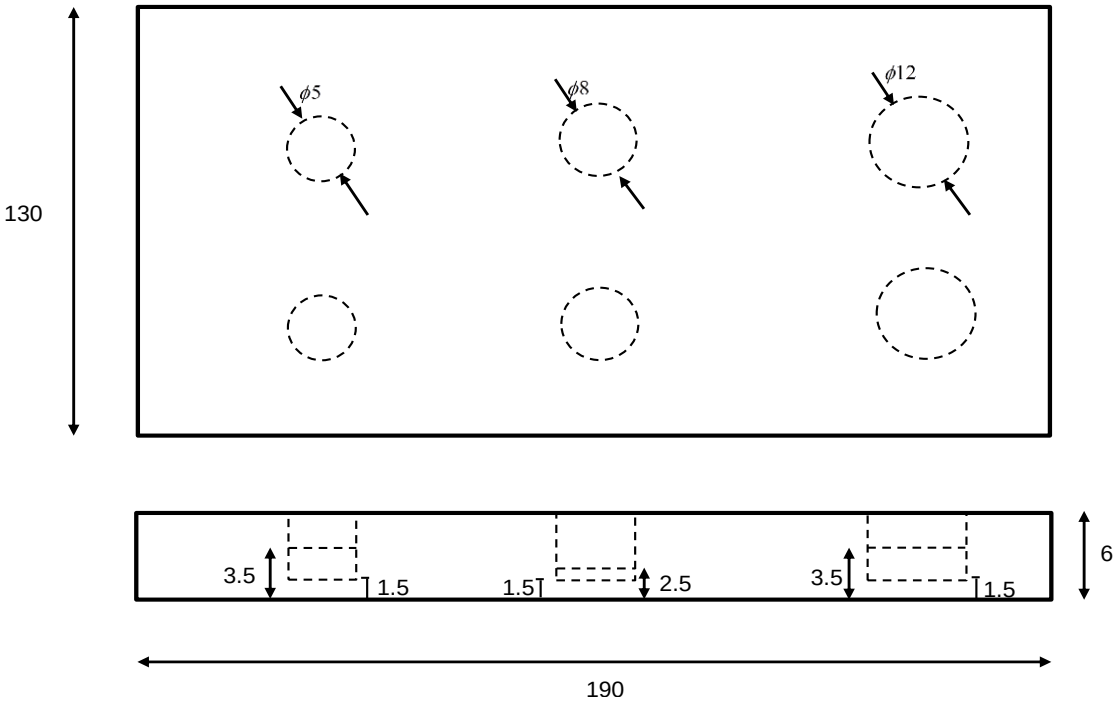

Figure 3-16. Geometry of the test specimen (units in mm)

3.3.1 Experimental Procedure of Pulse Thermography

Figure 3-17 illustrates the experimental set up of pulse thermography. The specimen was secured vertically on a wooden support. The camera was positioned $500mm$ away from the specimen The heating gun was switched on at low speed and hovered by hand on the front side of the specimen for $5s$ at an angle approximately 30^0 from the horizontal plane The Thermal camera recorded the change of temperature contrast on the surface of the specimen.

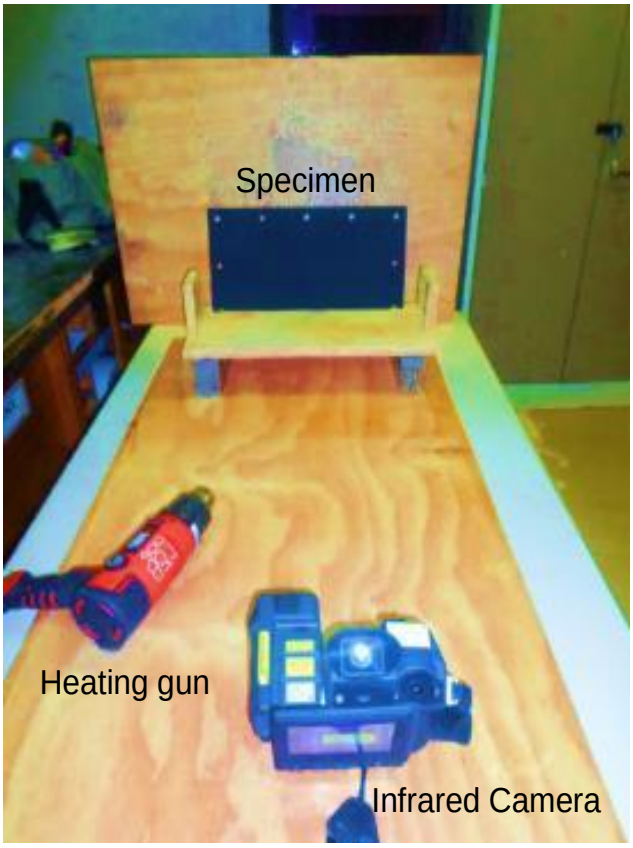

Figure 3-17. Illustration of equipment used during pulse thermography

3.3.2 Experimental Results

Figure 3-18 shows the rear or far side surface of the specimens. Figures 3-19, 3-20 and 3-21 are the thermal images on the near surface of the PVC, stainless steel and mild steel specimens after excitation. The presence of subsurface defects in all figures is noted by the circular hot spots.

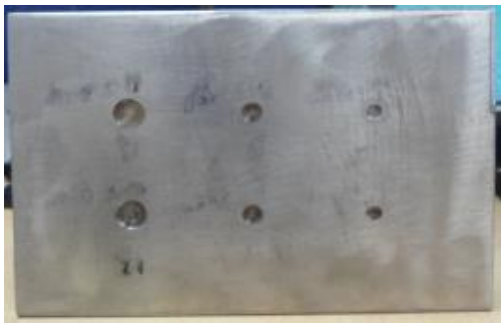

Figure 3-18. Rear view of the specimen with machined defects

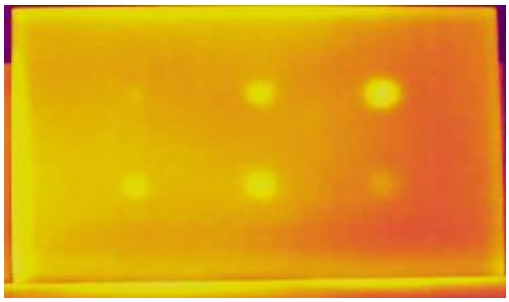

Figure 3-19. PVC specimen's results

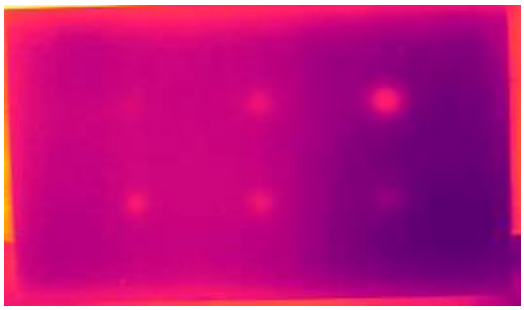

Figure 3-20. Stainless Steel specimen's results

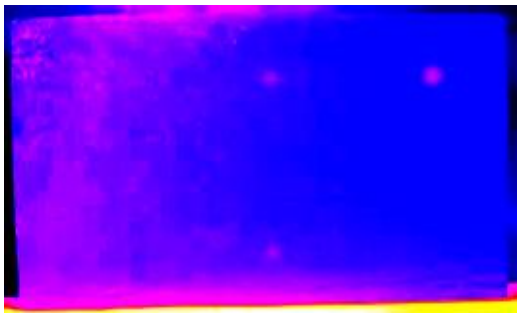

Figure 3-21. Mild steel specimen's results

3.3.3 Ultrasonic Testing

Ultrasonic testing was employed for the inspection of the specimens with the flat bottom holes which were previously examined using Pulse thermography. The test was performed in the UT laboratory at room temperature. A Kraukramer UT machine with a $5MHz$ Twin Crystal probe was used to detect the subsurface defects. An Ultrasound gel was used as a suitable coupling between the probe and the test specimen's surface. Figure 3-22 illustrates the UT experimental set-up.

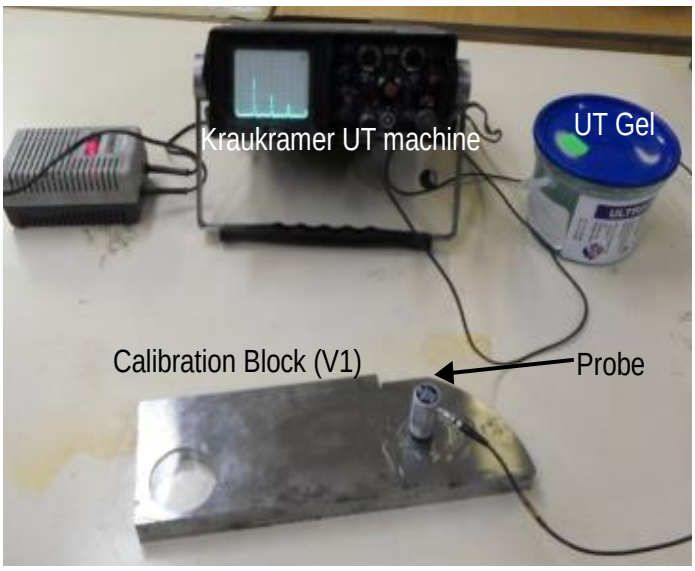

Figure 3-22. Ultrasound inspection set-up

3.3.4 Experimental Procedure of Ultrasound Test

The A-scan mode was used to display the amount of received ultrasonic energy as a function of time to estimate the relative discontinuity sizes by comparing the signal amplitude obtained from an unknown reflector to that of known reflector, and by the position of the signal on the horizontal sweep. The flat bottom holes (FBH) of each specimen in Figure 3-16 were given a unique alphabetic identification from A to F (see Figure 3-23). The Kraukramer UT machine was calibrated prior to the tests using a Standard Calibration Block (SCB) made from $25mm$ thick ferritic steel (V1), (see the calibration methods in Appendix D-1). The calibration was performed to create a linear display on the screen of the machine (see calibration results in Figure 3-24).

The inspected surfaces of the specimen were cleaned with the approved vapour degreasing cleaning agent to successfully remove loose rust, oil, grease and dust. The specimen was then placed on its far side on a flat surface. A digital camera was positioned to capture the results displayed on the screen of the UT machine.

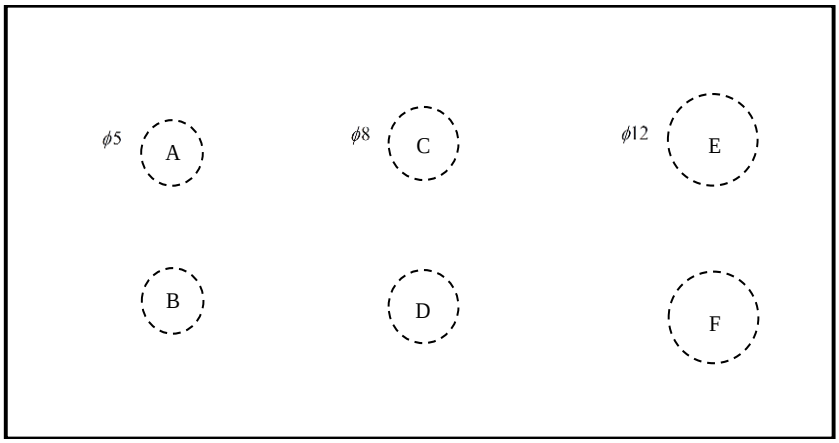

Figure 3-23. Alphabetic Identification of FBH in figure 3-16

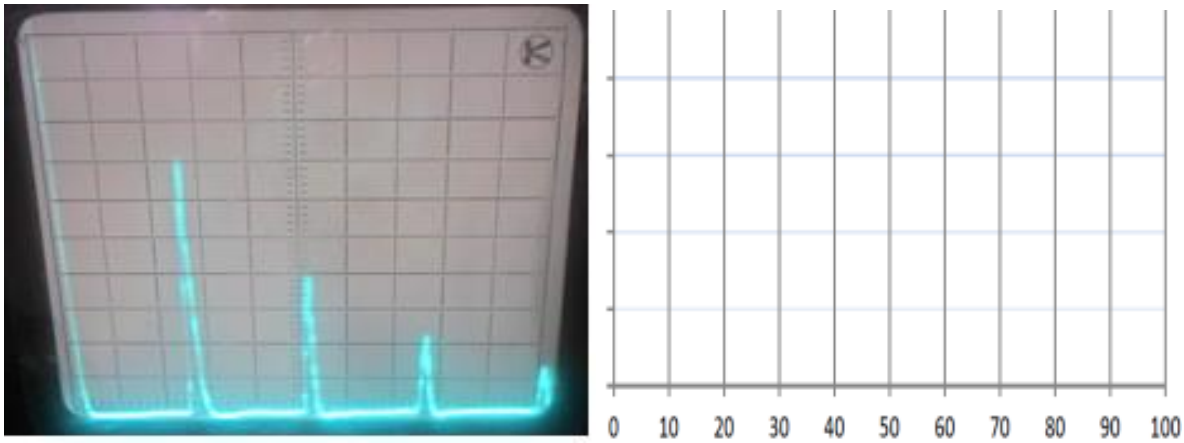

Figure 3-24. Calibrated Kraukramer Machine

3.3.5 Ultrasound Testing Results

Tables 3-1, 3-2 and 3-3 present the ultrasound results. Figure 3-25, 3-26 and 3-27 demonstrate echo of defects.

Table 3-1. PVC specimen's Ultrasound results

FBH	Actual Material Velocity (m/s)	FHB Depth (mm)	FBH Diameter (mm)
A	2312	1	6
B	2312	3	6
C	2312	2	8
D	2312	1.9	8
E	2312	1.5	12
F	2312	3	12

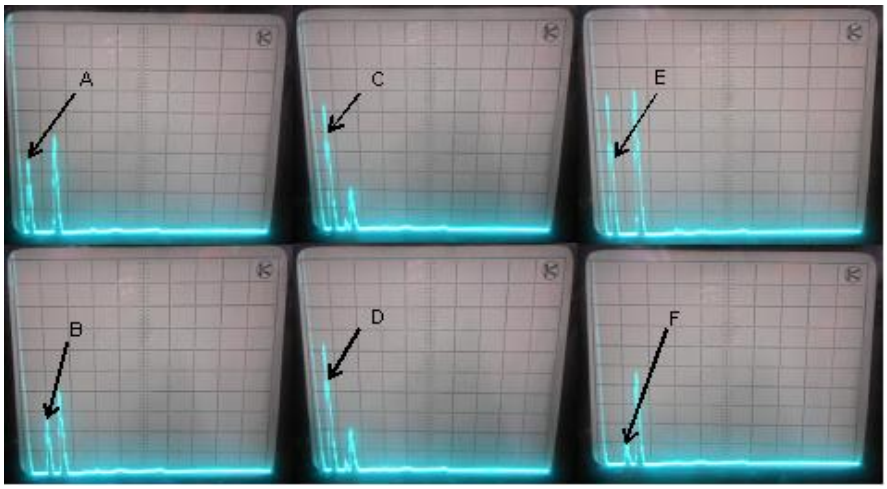

Figure 3-25. Echo of the PVC specimen's subsurface defects

Table 3-2. Stainless steel specimen's Ultrasound results

FBH	Actual Material Velocity (m/s)	FHB Depth (mm)	FBH Diameter (mm)
A	5850	1	6
B	5850	2	6
C	5850	1.3	8
D	5850	1.5	8
E	5850	2.5	12
F	5850	1	12

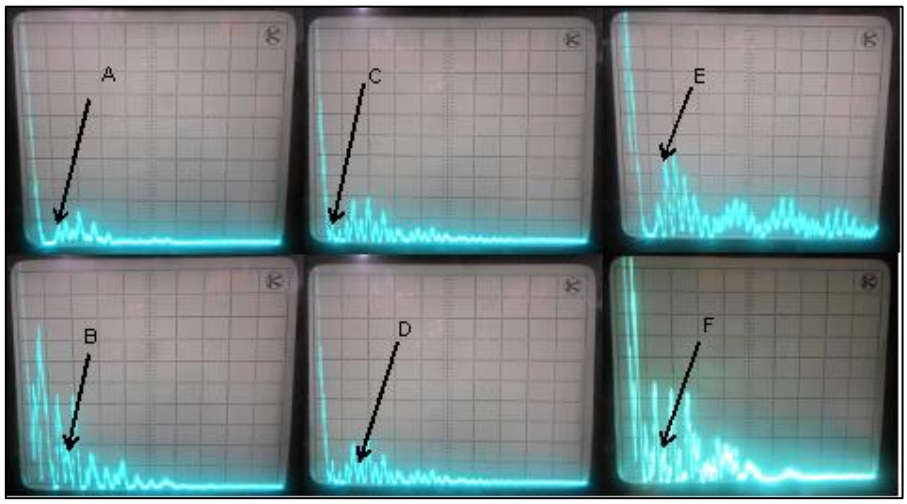

Figure 3-26. Echo of the Stainless steel specimen's subsurface defects

Table 3-3. Mild steel specimen's Ultrasound testing

FBH	Actual Material Velocity (m/s)	FBH Depth (mm)	FBH Diameter (mm)
A	5610	1	6
B	5610	2	6
C	5610	1.2	8
D	5610	1.5	8
E	5610	2.5	12
F	5610	1	12

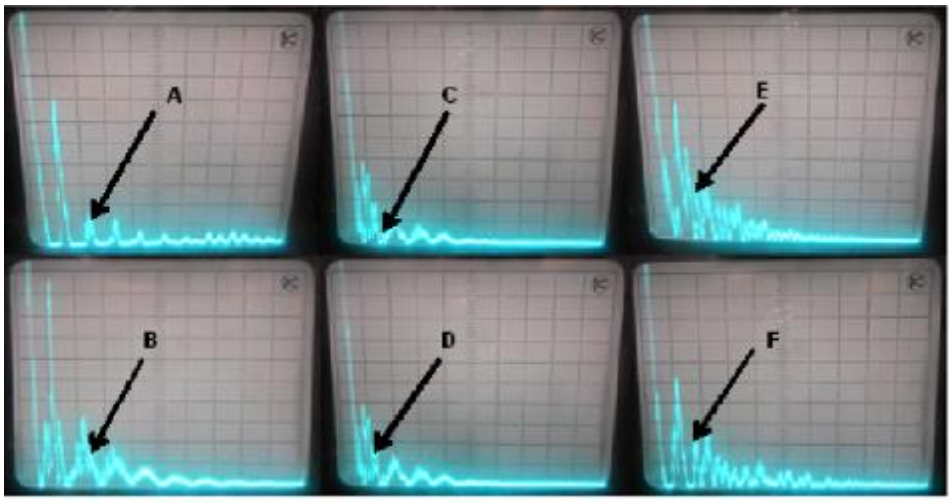

Figure 3-27. Echo of the Mild steel specimen's subsurface defects

3.4 Induction Thermography Methodology

The purpose of this study was to assess the effectiveness of induction thermography in detecting surface defects on a 304L stainless steel specimen, an HP turbine's stud (high-pressure turbine stud) and a CV-joint (constant velocity joint). The results of the technique were compared with those obtained through the traditional NDT techniques of MPI and DPI. Figure 3-28 is a typical induction thermography set up of the target (specimen), an induction conductor or coil, the AC-DC current generator and an infrared camera.

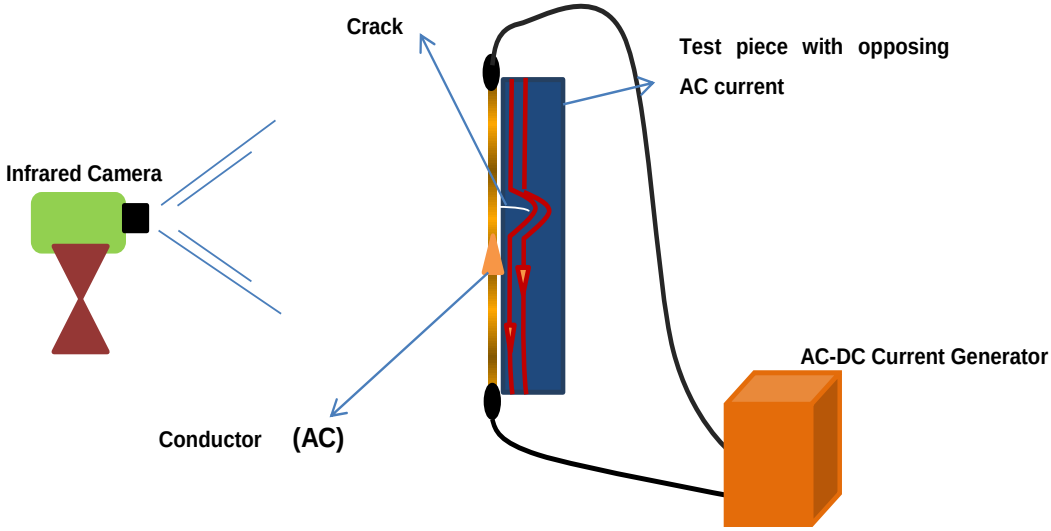

Figure 3-28. Schematic diagram of Induction Thermography

The 304L stainless steel specimen in Figure 3-29, was obtained from piping that had been removed from service due to the presence of stress corrosion cracking (SCC) that had developed over the course of many years. The presence of SCC on the pipes was identified by DPI. The specimen was cleaned using degreasing agent to remove the impurities. During the thermography experiment, the specimen was secured on a wooden support at 90^0 perpendicular to the horizontal surface.

Figure 3-30 depicts a specimen obtained from an M80 HP turbine stud (Material Specification Z12CNDV12.02) that was removed from service due to an indication of thermal embrittlement that developed between the threads over a period of $65{,}503 hours$ in operation in a $260^0 C$ environment. Prior to the inspection, the specimen was cleaned using a degreasing agent to remove impurities. The specimen was placed against the wooden bracket such that the inspected surface was perpendicular to the horizontal surface.

Figure 3-31 is a CV-joint that was removed from service for inspection, using MPI and DPI NDT techniques. The results indicated the presence of the defect on the shoulder of the joint (where the stub and housing joined). The CV-joint was subsequently inspected using Induction Thermography.

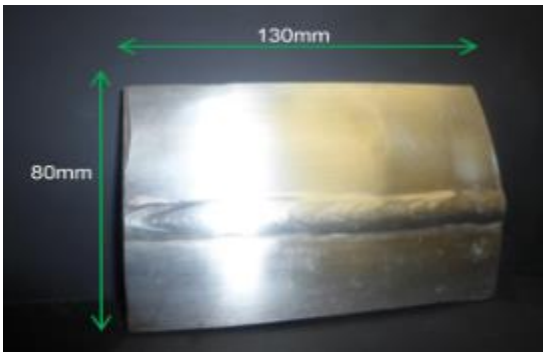

Figure 3-29. Typical 304L stainless steel test piece

Figure 3-30. Turbine's stud specimen

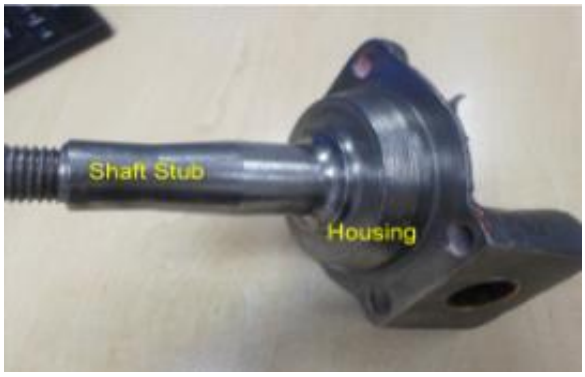

Figure 3-31. CV-joint

For the 304L stainless steel specimen and the HP turbine's stud, a straight conductor $400mm$ long was manufactured from $8mm$ copper tube. For the CV-joint an induction coil was manufactured from $6.23mm$ copper tube (see Figure 3-32). The conductor and coil were made to be mounted on a wooden bracket with the ends connected to the terminals of the AC-DC current generator.

Figure 3-32. Coil used for CV-joint inspection

A MAGNAFLUX AC-DC current generator was employed to generate the AC and DC currents. The generator had a maximum current of $1000Amps$, at a $50Hz$ frequency (depicted in Figure 3-33). A FLIR T640 thermal camera was used to monitor the temperature profile or temperature contrast along the entire test piece.

3.4.1 Research Methodology

Figure 3-33 is a typical experimental set-up for the Induction Thermography tests. During the experiments for the 304L Stainless steel and the HP Turbine's stud, the current generator was set to produce $400Amps$ alternating current, with the copper conductor connected to the terminals of the voltage supply cables. The conductor was placed parallel to the horizontal length of the specimen; the gap between the specimen and the conductor was set at $2mm$. The camera was set at a distance of $500mm$ facing the surface of the specimen. For 304L stainless steel, the conductor was powered for $30s$ and thereafter removed to avoid any reflections on the specimen which would affect the specimen's surface temperature profile.

The experimental set-up for HP turbine stud was similar to the one for the 304L stainless steel. The conductor was powered for $35s$ and thereafter removed to examine the stud thoroughly without obstruction/reflections.

The test performed on the shoulder of the CV-joint used the induction coil. The coil was fitted around the shaft stub of the CV-joint closer to the housing leaving a gap of approximately $3mm$. The current generator was set to produce $600Amps$ alternating current, with the copper conductor connected to the terminals of the voltage supply cables. The coil was powered for a period of $35s$ and thereafter removed to observe any indications of the presence of a defect on the shoulder of the CV-joint.

Figure 3-33. Typical experimental setup for Induction Thermography

3.4.2 Experimental Results

Figures 3-34, 3-35 and 3-36 are thermo-grams of the three 304L stainless steel specimens. On the left-hand side is a thermal image of the specimen before excitation, and on the right-hand side is a thermal image subsequent to induction heating.

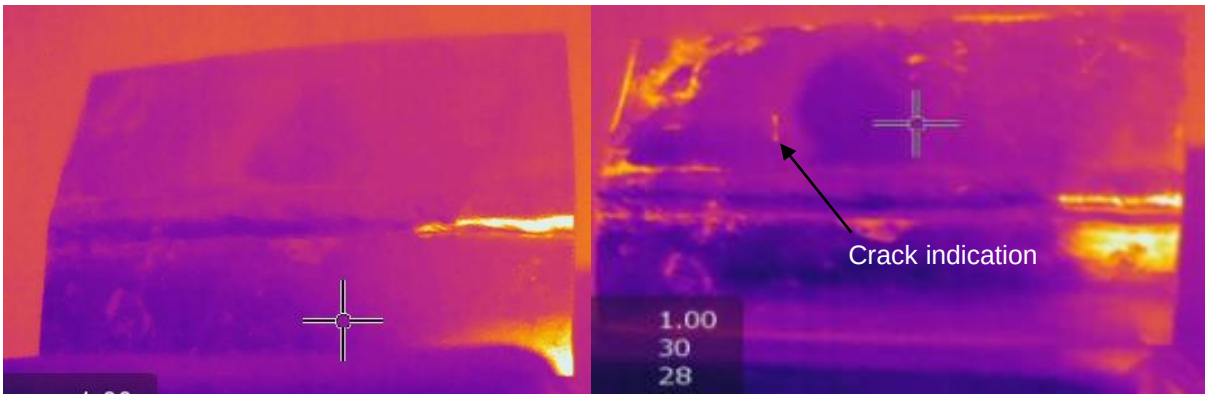

Figure 3-34. 304L stainless steel after excitation

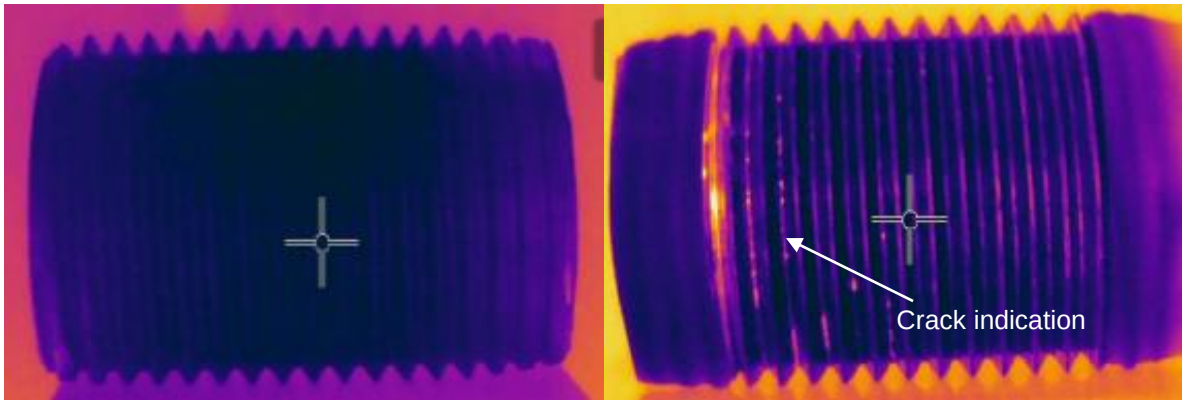

Figure 3-35. Results of M80 HP turbine's studs after excitation

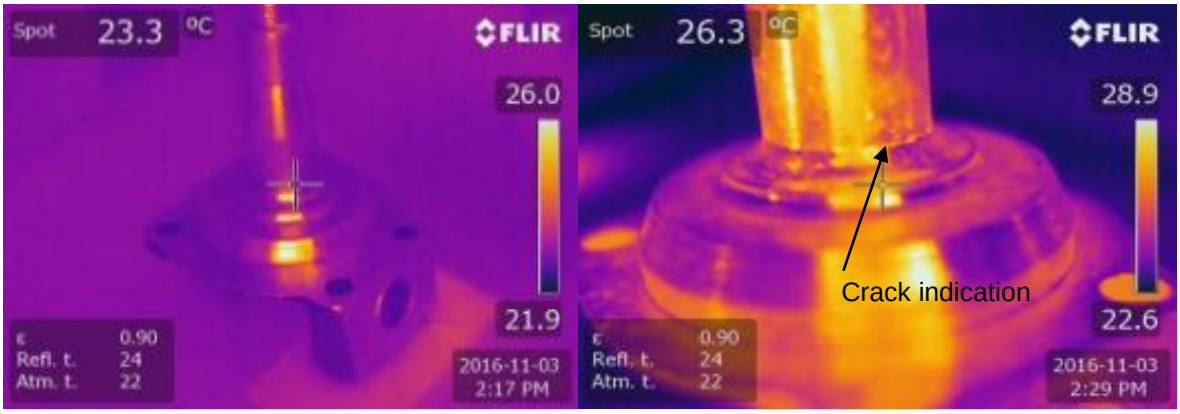

Figure 3-36. Results of CV-joint after excitation

3.4.3 Magnetic Particle Testing Methodology

Magnetic particle inspection was employed to inspect the HP turbine's stud and the CV-joint. The inspection was performed in a room with visible light (normal room light). A White Contrast Powder WCP-2 was applied on the surface of the specimens to provide a smooth high contrast background. An AC Articulated Y6 yoke was used to induce magnetism on the specimens by passing an electric current through them. The yoke used had C-shape electromagnets which induce a magnetic field between the poles (legs). The poles of the yoke are flexible and can be adjusted as required. Magnetic Particle Inspection ink 7HF was applied on the inspected surface during the magnetization of the specimens.

The specimen was cleaned with degreasing agent to remove the impurities such as oil, grease, loose rust on its surface. The surface of the specimen under inspection was sprayed with a WCP-2 prior to magnetization and wet particle application. The WCP-2 powder was allowed to dry completely before the magnetization. The yoke was placed on the surface of the specimen to induce current flow. The specimen was continuously magnetized while spraying the ink over its surface. The indications of the presence of a defect appeared as dark lines on white background.

3.4.4 Results of Magnetic Particle Inspection

Figure 3-37 depicts the stud during the MPI inspection. Figure 3-38 and 3-39 illustrate the results obtained during the Magnetic Particle Inspection technique on the HP turbine stud and the CV-joint.

Figure 3-37. Experimental set-up of MPI with the turbine's stud

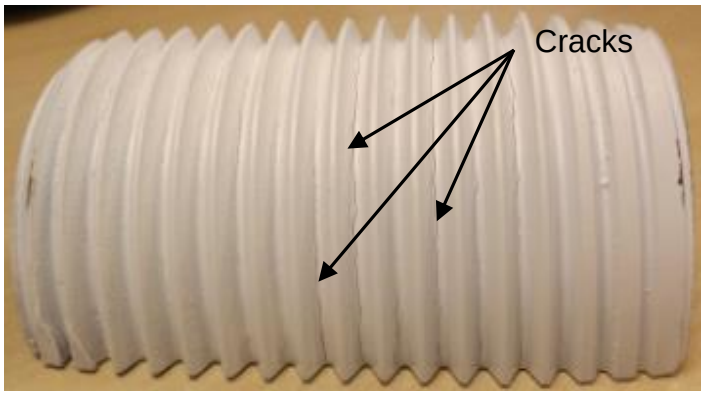

Figure 3-38. Turbine stud specimen

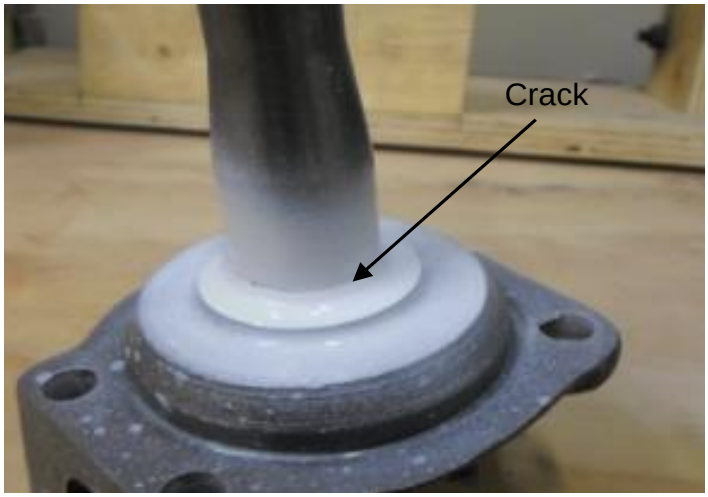

Figure 3-39. CV-joint from service

3.4.5 Dye Penetration Inspection

Dye penetration inspection was employed for detecting surface defects on the same specimens i.e. the 304L stainless steel plate, the HP turbine's stud and the CV-joint. The inspection was performed at room temperature. The DPI technique was successfully completed by employing the following three products. The first product used was red dye penetrant. The product was used to remove and clean the red dye penetrant on the surface of the specimen using a towel or cloth. The last product was a dry developer; this product was applied on the surface of the specimen where it forms a white dry thin layer to absorb the penetrant inside the cracks.

The inspected surfaces of the specimens were cleaned with approved vapour degreaser cleaning agent to successfully remove loose rust, oil, grease, clog cracks which can prevent the penetrant from filling the voids on the surface. The surface of each specimen was

sprayed with red dye penetrant and allowed a period of $15\,\mathrm{min}$ to penetrate through the cracks. After the waiting period, a paper towel was sprayed with dye penetrant remover and the specimen's surface was cleaned and dried. The dry developer was shaken to restore fully the white developer particles suspension. On a dry surface, the dry developer was applied and allowed it to absorb the red penetrant between cracks. The developer was allowed to dry completely to allow indications to reach their full pattern. Cracks were indicated by red lines. On completion, the developer was removed by using a dry towel.

3.4.6 Results of Dye Particle Inspection

Figures 3-40, 3-41 and 3-42 illustrate the results obtained during the dye penetration Inspection on the 304L stainless steel plate, the HP Turbine's stud and the CV-joint.

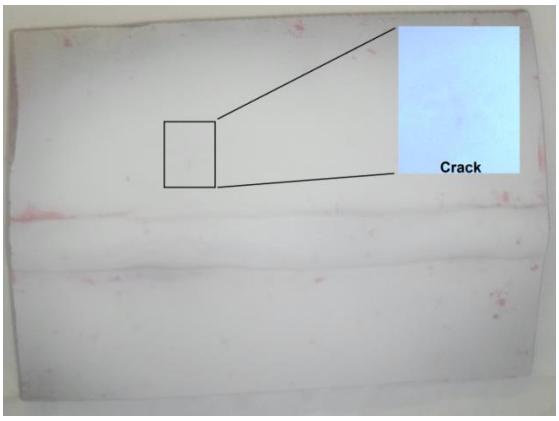

Figure 3-40. DPI results from the 304L stainless steel test piece

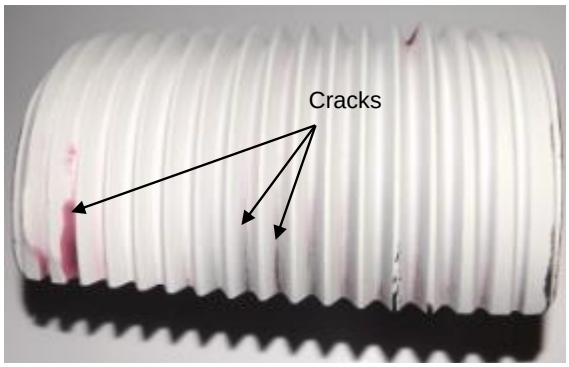

Figure 3-41. DPI results from the HP-turbine's stud specimen

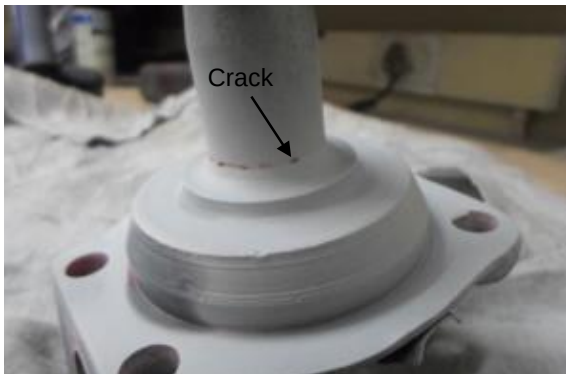

Figure 3-42. DPI results from the CV-joint

CHAPTER 4: DISCUSSION AND CONCLUSIONS

4.1 Introduction

In this chapter, the author develops a discussion and arrives at conclusions regarding the experimental results obtained when attempting to introduce IRT as yet another NDT technique in the mechanical maintenance arena. Following is a treatise on the results obtained from the internal leak inspection, pulse thermography and induction thermography experiments, encompassing the comparison with the results obtained through the traditional of MPI and DPI techniques, and the conventional of UT.

4.2 Internal Leak Inspection

Infrared Thermography was successfully demonstrated as a tool to detect internal leaks in piping networks. The success of the technique was observed on the results which were clear to interpret. Leaking valve(s) were identified by the change of thermal energy (surface temperature) of the pipe downstream. Pipes downstream of a leaking valve had greater thermal energy than those without a leaking valve. IRT successfully presented the change of thermal energy in the thermal images that were produced. This condition was also observed by Matthew [10 and 43] when investigating internal leaks through passing valves, steam traps, and safety valves in the American Electric Power (AEP) plants.

The change of thermal energy cannot be seen by naked eye, however, IRT detects the electromagnetic energy released by the pipes' surface and converts it to visual thermal images, for an operator to differentiate between leaking and non-leaking valves.

The results from this technique are basically qualitative since it currently cannot quantify the amount of fluid leaking through the valve. According to Sulaiman [13], the technique requires numerical intervention to obtain quantitative results. The technique cannot be used in a system where the fluid is at ambient temperature.

4.3 Pulse Thermography

In this study, pulse thermography was successfully demonstrated as non-contacting NDT technique that can be used to detect subsurface defects in PVC, stainless steel, and mild steel materials. The results obtained from the study were clear and understandable. IRT detected subsurface defects (flat bottom holes beneath the surface) as circular hot spots on the surface of the specimen (see Figure 3-20, 3-21 and 3-22). The appearance of the hot

spots after excitation was similar to the results obtained by Suman at al [21], Stefano *et al* [30] and Reza *et al* [44] based on the scientific principle mentioned by Sheregii [23], briefly described in chapter 2 (2.3.1) of this dissertation.

The PVC specimen's thermal images displayed the greater thermal contrast, followed by the ones from the Stainless steel and Mild steel in that order (see Figure 3-23). The thermal contrast is influenced by the thermal diffusivity of the material [20, 23, 24 and 25] (see also Equation 6) which in turn depends on its thermal conductivity, specific heat capacity, and density. As seen in Table 4-1 the PVC material has the lesser value of thermal diffusivity. The results of this particular aspect of this study are similar to those obtained by Almond *et al* [24], while performing an analysis of the delamination detection capability of the pulse stimulated thermographic non-destructive testing technique with five materials (Aluminum alloy, Mild steel, Stainless Steel, Carbon fiber and Glass reinforced plastic) inspected for subsurface defects. In their study, the carbon fiber specimen produced the greater thermal contrast compared to the other materials because of its lesser value of thermal diffusivity.

Table 4-1. Material properties of the specimens used in this study

Material	**Thermal Conductivity** $\left(Wm^{-1}K^{-1}\right)$	**Specific heat** $\left(Jkg^{-1}K^{-1}\right)$	**Density** $\left(kgm^{-3}\right)$	**Thermal diffusivity** $\left(m^2s^{-1}\right)$
PVC	0.19	900	1.467	0.08×10^{-6}
Stainless steel	13.4	468	8230	3.47×10^{-6}
Mild steel	64	434	7830	18.8×10^{-6}

The results suggest that the thermal contrast is also influenced by both the size and the depth of the defect. Defects close to the surface appeared to have greater thermal contrast than defects in deeper/greater depth, also defects with greater size have greater thermal contrast than small defects. This is in accordance with the conclusions by Sheregii [23] and Clemente [45], who conducted studies of detecting hidden defects using infrared

thermography varying the size and depth of the defects. The smallest defects that could be detected in this study was $5mm$ diameter and $3.5mm$ from the surface.

4.4 Magnetic Particle Inspection

The inspections performed on the HP turbine stud and the CV-joint using Magnetic Particle Inspection was conducted successfully with clear and easy results to interpret. Black oxide on the HP turbine stud was the indication of crack present on the roots of the threads. On the CV-joint an indication of a crack was observed on the shaft stub and housing. As mentioned by Mark *et al* [34], the presence of a crack was noted by the collection of iron fillings. These results are similar to those obtained by Luk et al [33] when performing a study on human factors and ergonomics in dye penetration and magnetic particle inspection methods on the welded mild steel plates.

4.5 Dye Penetrant Inspection

The Dye Penetrant Inspections on 304L stainless steel, HP turbine stud and CV-joint were performed successfully. The results obtained were similar to those obtained/presented by [32, 33 and 34]. On the 304L stainless steel plate there was a hair line crack on the left hand side of the centre above the sim-weld and corrosion pitting on its surface. On HP turbine stud, crack indications were observed on the roots of the threads, and on the CV-joint a crack was noted where the shaft stub joins the housing..

4.6 Ultrasound Testing

The results obtained from the inspection of PVC, stainless steel, and mild steel specimens were clear and easy to understand. PVC specimen had clearer noise levels as compared to that of stainless steel and mild steel. All six defects at different depth were detected. Both qualitative and quantitative results could be obtained with ultrasound testing. The results obtained are similar to those obtained by Olivier et al [42] when simulating the probability of detecting flat bottom holes within seamless steel pipes.

4.6.1 Comparison between Pulse thermography and Ultrasound Testing

In terms of size and depth from the inspecting surface Pulse Thermography mainly provides qualitative results, whereas Ultrasound Testing provides qualitative and quantitative results. Pulse thermography as a non-contacting technique is capable of fairly quickly inspecting large surface areas, whereas with Ultrasound testing a fair amount of time is required in scanning large surfaces. In cases where a large surface is to be inspected and requires qualitative and quantitative results, it would be preferable for both techniques to be

employed. Pulse thermography to locate the defects and Ultrasound testing to quantify them. The results of this comparison are similar to that obtained by Suhas [14], where Pulse thermography was compared with Ultrasound technique for inspection of adhesively bonded structures. Both techniques were found to be useful and complement each other as mentioned in this study.

It is concluded that Pulse Thermography can be used to provide qualitative information (i.e. the presence) of subsurface defects on PVC, stainless steel, and mild steel materials.

4.7 Induction Thermography

This study demonstrated that induction thermography can be employed in the mechanical maintenance program for inspection of surface defects on metals. The presence of defects (cracks) was made visible by an increase of temperature distribution at the defect. The IRT showed the intensity of the heat at the defects as a temperature contrast compared to areas without defects (see Figure 3-36, 3-37 and 3-38). The temperature contrast produced by the defect was also observed by Goldammer *et al* [46] when inspecting the rotor wedges of a power generator using induction thermography. According to Vrana *et al* [27], the heat intensity at the defect was caused by the high concentration of current density around the defect.

The thermal profile of the defects (cracks) obtained in this study and by Patrick *et al* [47], Topelas *et al* [48] and Maillard *et al* [49] appeared as a solid line with heat intensity on the entire crack, different from the results obtained by Ruizhen *et al* [50], Jia *et al* [51] and Jianping *et al* [52] where the heat intensity concentrated at the edges of the cracks. According to Vrana *et al* [27], the thermal profile depends on the type of crack. Open cracks will generate intense heat at the edges while close cracks will have a series of heat intensity in the form of dots due to contact bridge effect which might look like a solid line. However, an increase in current density can influence both scenarios to have a solid heat intensity as a line.

The technique is limited to metallic components. The thermal contrast created by the defect does not reveal any reliable or exact geometrical information in terms of the defect's size but perhaps an approximation.

4.7.1 Comparison between Induction Thermography and MPI

In this study induction thermography and magnetic particle inspection (MPI) were used to inspect an HP turbine stud and a CV-joint. Both techniques could detect most of the defects between the threads of the HP turbine stud, however, with Induction thermography 8 defects

between threads were identified, whereas with Magnetic Particle Inspection 7 defects could be identified. During the inspection of a CV-joint, both techniques could detect the crack between shaft stub and housing. However, induction thermography inspection provides clear contrast indications of defects than Magnetic Particle Inspection. Induction Thermography as a non-contacting technique is capable of inspecting large surface areas, whereas MPI is more suited to inspect small areas. Patrick *et al* [6], reported on induction thermography and magnetic particle inspections on 26 wheel hubs. The results indicated that induction thermography revealed more defects and could detect radial and circumferential defects effectively, whereas MPI could hardly detect circumferential defects. Udo *et al* [53] claimed that induction thermography is a fast non-contacting NDT technique even for complex shaped metallic components and a suitable alternative to MPI.

4.7.2 Comparison between Induction Thermography and DPI

With induction thermography defects were observed in 304L stainless steel, the HP turbine stud, and CV-joint, whereas dye penetration inspection could only reveal defects on the HP turbine stud and CV-joint. DPI could not reveal most of the defects between the threads of the HP turbine stud as compared to that revealed by induction thermography. However, both techniques could clearly indicate the defect between the shaft stub and housing of a CV-joint. The waiting period to obtain the results when using DPI was approximately 15minutes longer as compared to induction thermography when performing inspections on 304L stainless steel, the HP turbine stud, and CV-joint. Both techniques can be used to detect large surface areas, however, induction thermography is quicker than DPI. Goldammer *et al* [46] said the inspection of rotor wedges required up to 20 days with DPI, however, with induction thermography it was reduced to 5 days.

The results indicate that induction thermography is a potential alternative or replacement of the traditional MPI and DPI techniques for the detection of surface defects/flaws (see comparison images in Appendix F).

This study demonstrated that infrared thermography can be introduced successfully as a non-destructive technique in the mechanical maintenance arena.

4.8 Conclusion

The main objective of this study was to compare the effectiveness of detecting defects using infrared thermography with those achieved using traditional/current NDT techniques in the mechanical maintenance areas of interest in a power plant.

Three aspects of thermography were employed; Passive thermography was successful in detecting internal leaks through isolation and safety valves. The technique was experimented with a model in the laboratory and tested in real plant conditions.

The effectiveness of Induction Thermography became apparent when inspecting for surface defects on electromagnetic materials, such as 304L stainless steel plate, a M80 HP turbine stud and a CV-joint. The results obtained were similar to those obtained by the traditional NDT techniques of MPI and DPI.

Pulse Thermography, (the third technique) was successful in detecting subsurface defects (flat bottom holes) on specimens made of materials such as PVC, Stainless steel, and Mild steel.

The results from these three infrared thermography techniques assisted in concluding that considerable progress has been achieved in terms of qualitative defect detection, however there are still disadvantages in terms of characterization of the defects.

4.8.1 Future Work

Future work in order to enhance the use and effectives of the abovementioned infrared thermography techniques, should perhaps cover the following aspects:

- With regards to internal leaks inspection; This study reviewed the principle on pipes without lagging/insulation. Therefore, to eliminate the task of removing lagging before inspection a study needs to be conducted to ascertain the effectives of IRT with lagging fitted on pipes.
- The implementation of remote or robotic systems to inspect equipment with induction thermography and pulse thermography.
- The improvement of thermography equipment toward finite pulse times excitation to detect smaller defects.

APPENDICES

Appendix A. Infrared Camera

Table A.1. Infrared Camera Specifications

Features	FLIR T640
Field of view /Minimum focus distance	25^0 x 19^0 / 0.25m
Thermal sensitiveness	<0.035^{0}C @+30^{0}C
Image frequency	30Hz
Focus	Automatic or manual
Zoom	1-8 x continuous, digital zoom, including panning
IR resolution	640 x 480 pixels
Display	Built-in Touch-screen
Viewfinder	Built-in 800 x 480 pixels
Picture-in-Picture	Resizable and movable IR area on visual image
Temperature range	-40^{0}Cto+150^{0}C,+100^{0}C to +650^{0}C,+300^{0}C to +2000^{0}C
Accuracy	±2^{0}C or ±2% of reading
Weight	1.3kg
Size (L x W x H)	143 x 195 x95mm
Tripod mounting	UNC $1/4''$ -20
Battery Type	Li-Ion / 2.5 hours, Display show battery status
Charging system	In camera AC adaptor / 2bay charging system

Appendix B. Dimensions and material used to manufacture the FHS

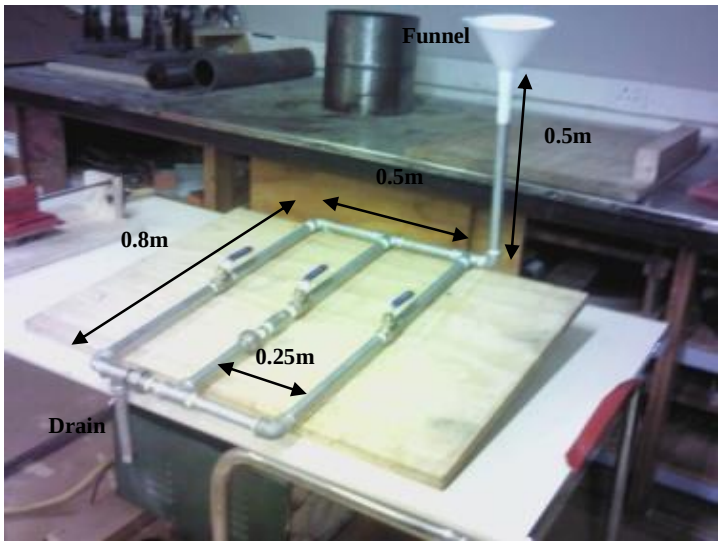

Figure B.1. Dimensions of the model system

Table B.1. Material to manufacture the FHS

Item Description	Diameter Size (mm)	Quantity
Pipe	12.7	3m
Barrel Nipple	12.7	1
Union	12.7	1
Socket	12.7	1
90^0 Elbow	12.7	2
90^0 Elbow Male/Female	12.7	2
T-Piece	12.7	4
Thread Seal Tape (PTFE)	12.7x4.6	1 x roll
Reservoir (Funnel)	-	1

Appendix C. Procedure to measure the emissivity

SCOPE

- This procedure is to demonstrate how to calculate the emissivity of material using infrared thermography.

PURPOSE

- Is to calibrate the thermal imager (camera) with the same emissivity as the specimen, this is to prevent incorrect readings during the experiment.
- To eliminate other material in the area with high thermal energy than the specimen under test.

EQUIPMENT USED

- Material/Equipment to be measured.
- Infrared Camera FLIR T640
- Black electric insulation tape

PROCEDURE

1. Place the camera on a flat supporting devise, 500mm from the test piece.
2. Point the beam of the camera at the centre of the specimen.
3. Measure the temperature of an object T_{obj}, and record it .....
4. Modify the surface to black body surface, by applying a piece of insulation tape on the specimen where the camera is pointing.
5. Measure the temperature of a blackbody $T_{blackbody}$, and record it .....
6. Manually calculate the emissivity using equation 1 and 3 for body and black body energies, then substitute these values into equation 2 for emissivity.
7. Repeat the procedure at least for three times and obtain the average.
8. Enter the average value of the emissivity obtained in the parameters of the camera.

Appendix D. Calibration of Kraukramer UT machine using V1 block

SCOPE

- This procedure demonstrates the calibration of Kraukramer UT machine with a 5MHz Twin Crystal probe using a V1 calibration block.

PURPOSE

- To ensure that the UT machine is accurate and performs as designed.

EQUIPMENT USED

- V1 Calibration Block (25mm thick side)
- Kraukramer UT machine
- 5MHz twin Crystal probe
- Ultrasound testing gel

PROCEDURE

1. Ensure the machine is powered
2. Connect the probe to the machines
3. Lay the V1 block flatwise, and use 25mm thick side.
4. Apply gel on the surface of the block.
5. Couple the probe to the V1 block, see Figure 3-22, and the back-wall echo sequence now comes from the 25mm steel path.
6. Adjust the echoes from the calibration block using Pulse shift as well as Coarse and Fine ranges. See desired results in Figure 3-24.

Appendix F. Induction Thermography Comparison Images

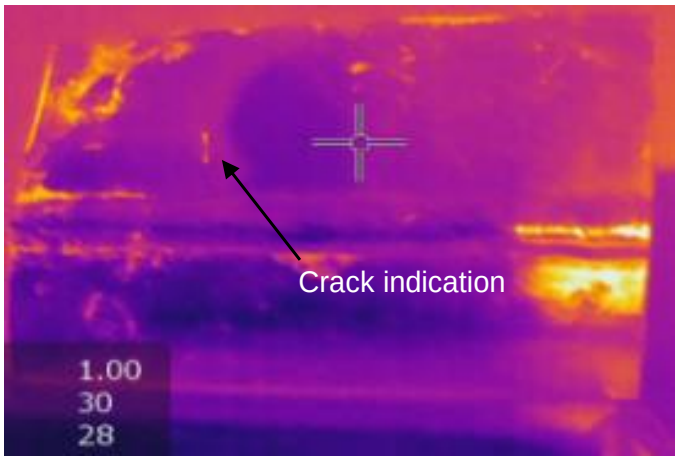

(A) Induction Thermography

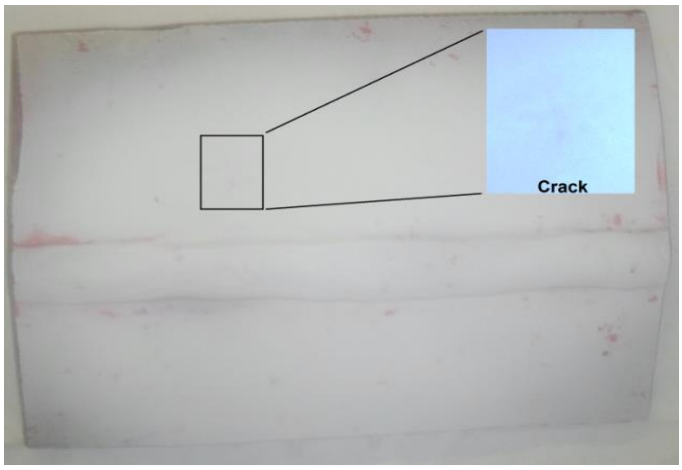

(B) Dye Penetration Inspection

Figure F-1. 304L Stainless Steel Comparison Results

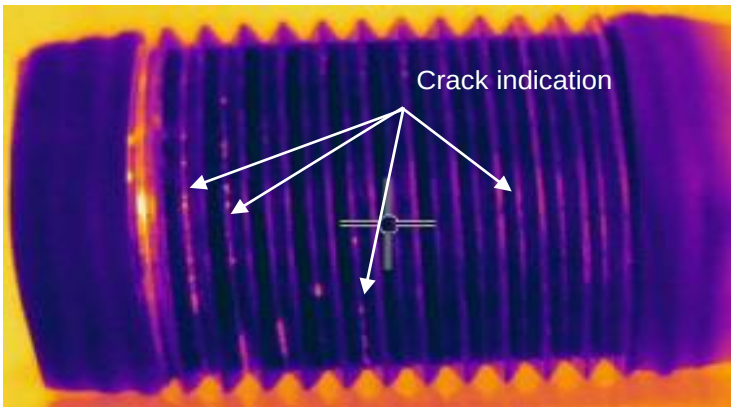

(A) Induction Thermography

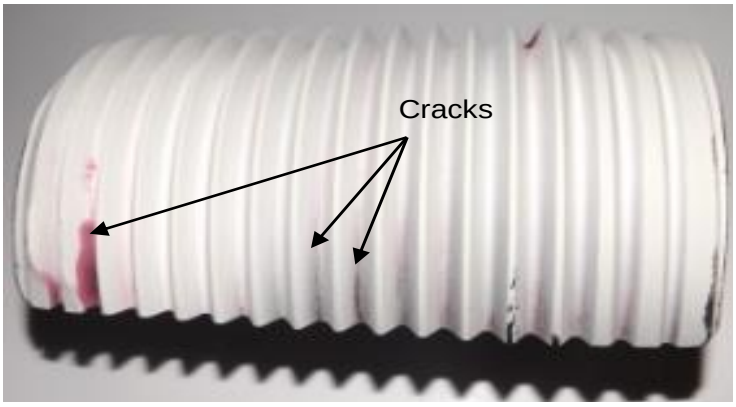

(B) Dye Penetration Inspection

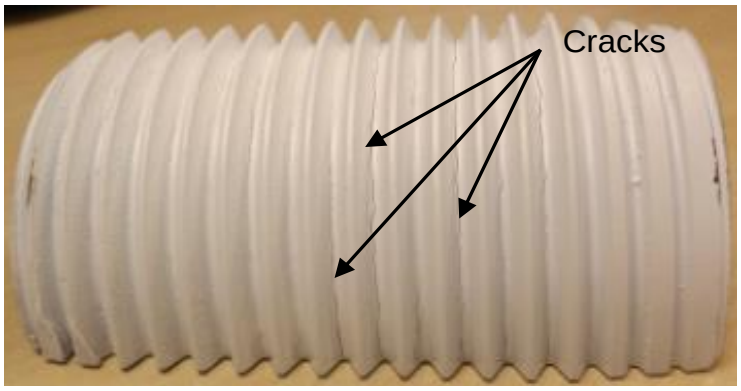

(C) Magnetic Particle Inspection

Figure F-2. M80 HP Turbine Stud Comparison Results

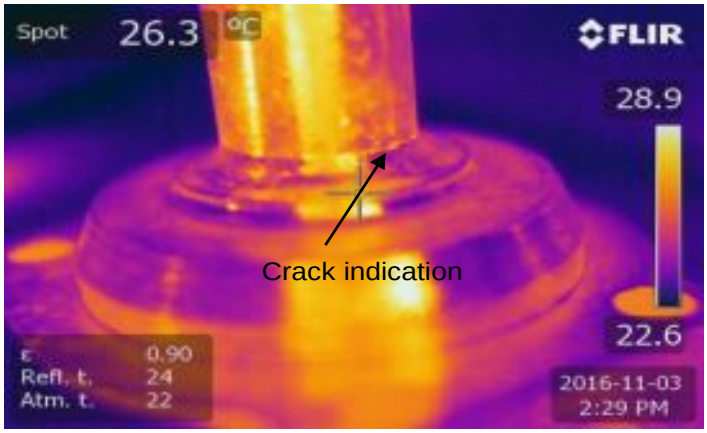

(A) Induction Thermography

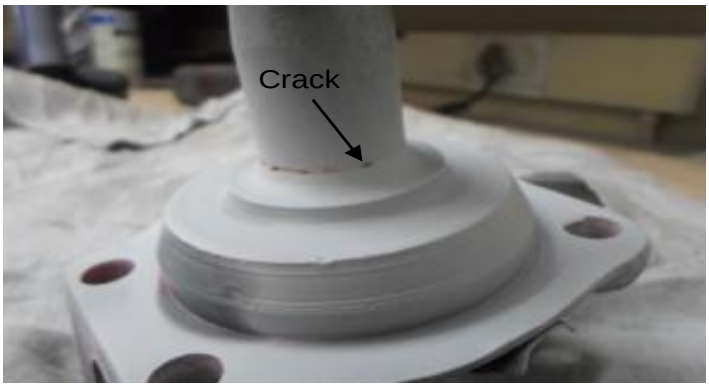

(B) Dye Penetrant Inspection

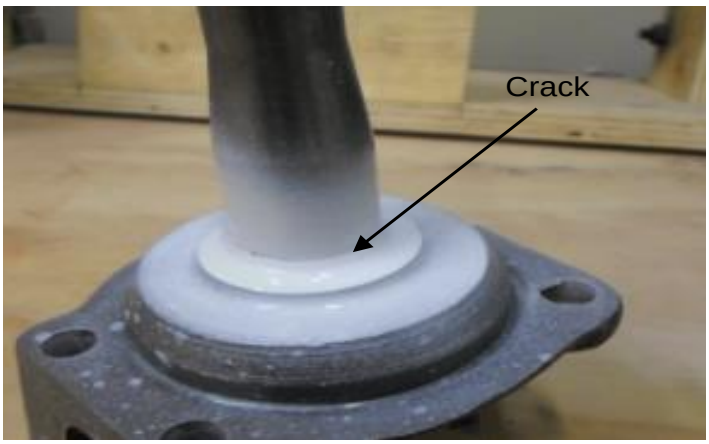

(C) Magnetic Particle Inspection

Figure F-3. CV-Joint Comparison Results

BIBLIOGRAPHY

[1]. A. S. Nazmul Huda, S. Taib, Application of infrared thermography for predictive / preventive maintenance of thermal defect in electrical equipment. *Applied Thermal Engineering*, 2013, 61, pg. 220-227.

[2]. U. Ruben, V. Publo, G. Jon, V. Laura, M. Julio and G. B. Francisco. Infrared Thermography for Temperature Measurement and Non-Destructive Testing. *Sensor*, 2014, 14, pg. 12305-12348.

[3]. F. Dirk, J. Gryzagoridis, C. Lombe. Comparing Infrared Thermography and ESPI for NDE of Aircraft Composites. *Researchgate*. 20 May 2014. Available from: http://www.researchgate.net/profile/Jasson_Gryzagoridis/publication/233683995_Comparing_infrared_thermography_and_ESPI_for_NDE_of_aircraft_composites/links/00b49532e7801842dd000000.pdf. [Accessed 20 May 2015].

[4]. M. M. Rodríguez, S. Lagüela, A. D. González, P. Arias. Cooling analysis of welded Materials for crack detection using infrared thermography. *Infrared Physics & Technology*, 2014, 67, p. 547-554.

[5]. M. Xavier. sa. Applications of Infrared Thermography in Non-destructive Evaluation. *Electrical and Computing Engineering Dept*. Available from: http://w3.gel.ulaval.ca/~maldagx/r_1123.pdf [Accessed 20 May 2015]

[6]. B. Patrick, L. Gregory, M. Samuel, C. Julien and L. B. Jean. Induction Active Thermography as an alternative to Magnetic Particle Inspection. *11th International conference Qualitative Infrared Thermography*, held in Naples, Italy on 11-14 June 2012.

[7]. M. Vasyl. Infrared Radiation. 1st edition. *Intec, 2012*, X. Preface.

[8]. M. Xavier. Infrared Thermography for NDT: Potential and Applications. *INSA LYON*. Universite LAVAL, 9 November 2013.

[9]. P. Vladimir, M. Marijan, and K. Dudravko. Infrared Thermography in Marine Application. *Otvoreno za raspravu*, 2008, 59 (2), p. 123-130.

[10]. C. Matthew. Leak Detection with Thermography & Ultrasonic acoustic. Plant Engineering Programme. 30th October – 4th November 2006.

[11]. A.E. Rozlosnik. Infrared thermography and ultrasound for both testing and analysing valves. In *Aerospace/Defense Sensing and Controls,* 1998, March, p (137-153). International Society for Optics and Photonics.

[12]. J. R. Michael, Power Plant Thermography - Wide Range of Application. *InfraMatiom*, Exelon Nuclear, LaSalle Station, 104A, 27 July 2004.

[13]. Sulaiman. Determining Internal Leakages of High Pressure and Temperature Steam Valve

[14]. V. Suhas. Studies on Infrared Thermography and Ultrasonic Inspection of Adhesive Bonded Structures, Overview and Validity. MSc Thesis, Clemson University, August 2010.

[15]. G. Xingwang and V. Vladimir. Crack detection in aluminium parts by using ultrasound-excited infrared thermography. *Infrared Physics & Technology*, 2013, 61, pg.149-156.

[16]. P. Bouteille, G. Legros, H. Walaszek, Comparison between Induction Thermography and conventional NDT Methods for Forged Parts, 11th European Conference on NDT, October 2014.

[17]. J. W. Norman. *Principles and Practices*, Vol 1. England: The British Institute of Non-Destructive Testing, 2004, pg. 1 - 2.

[18]. T.D. Eastop, A. McConkey. Applied Thermodynamics for Engineering Technologists, 5th edition. England: Pearson Prentice Hall, 1993, pp. 561 - 652.

[19]. C. L. Clemente, R. T Jose and P. V. M. Xavier. Non-destructive Testing with Thermography. *European Journal of Physics*, 2013, 34(6), pg. S91 - S109.

[20]. F.J. Francisco, I.C. Clemente, M.C. Olga, M. P. V. Xavier, M. L. Jose, Enhanced contrast detection of subsurface defects by pulsed infrared thermography based on the fourth order statistic moment, kurtosis, 2009, Vol. 7299.

[21]. T. Suman, A. Aparna, G. Ripul, K. Satish, H.K. Sardana and M. Ravibabu, Detection of subsurface defect using active infrared thermography.

[22]. W.B. Larbi, C. Ibarra-Castanedo, M. Klein, A. Bendada and X. Maldague, Experimental comparison of lock-in and pulsed thermography for the nondestructive evaluation of aerospace materials. In *6 th International Workshop, Advances in Signal Processing for Non Destructive Evaluation of Materials (IWASPNDE),* Ontario, Canada. Citeseer. 2009, August.

[23]. E.M. Sheregii. Thermography detection of hidden defects. Centre of Microelectronics and Nanotheology. 2015. Vol 4. pg. 31-35.

[24]. D. P. Almond and S. G. Pickering. Analysis detection of the delamination capabilities of pulsed stimulated thermography non-destructive test techniques. Material evaluation, 2014-January, pg. 79-86.

[25]. G. Wróbel, Z. Rdzawski, G. Muzia and S. Pawlak, 2009. Determination of thermal diffusivity of carbon/epoxy composites with different fiber content using transient thermography. *Journal of achievements in materials and manufacturing engineering*, *37*(2), pp.518-525.

[26]. S. P. Grzegorz. Studies on Investigation and Development of Transient Thermography for Detection of Disbonds in Thermal Barrier Coating Systems. Dr Eng Thesis, Imparial College London, December 2012.

[27]. J. Vrana, M. Goldamme, J. Baumann, M. Rothenfusser and W. Arnold.

Mechanisms and Models for Crack Detection with Induction Thermography. *Review of Quatitative Nondetructive Evaluation*, 2008, 27, pg. 475 - 482.

[28]. J. Vrana, M. Goldamme, K. Bailey, M. Rothenfusser and W. Arnold, Induction and Conduction Thermography: Optimizing the Electromagnetic Excitation towards Application. *Review of Quatitative Nondetructive Evaluation*, 2009, Volume 28, pg. 518 - 525.

[29]. J. Peng, G. Yun Tian, L. Wang, Y. Zhang, K. Li, X. Gao, Investigation into eddy current pulsed thermography for rolling contact fatigue detection and characterization, NDT&E International, Volume 74, May 2015, Pages 72-80, ISSN 0963-8695.

[30]. S. Stefano, P.A. Nicolas, I.C. Clemente, S. Carlo, T. Panagiotis, B. Abdelhakim P. Alfonso, P. Domenica, K Maria and M. Xavier. Surface and Subsurface Defects Detection in Impacted Composite Materials Made by Natural Fibers, Using Non-destructive Testing Methods, International Journal Composite Material, 2014, 4(5A), pg.1-9.

[31]. T Astrom. Use of Non-destructive Testing in Engineering Insurance. *IMIA WGP*, Fineland, 2002.

[32]. International Atomic Energy Agency. Liquid Penetrant and Magnetic Particle Testing at Level 2, IAEA Training course series no. 11, Austria: Vienna International Centre, 2000.

[33]. B. L. Luk, H. S. Alan and Chan, Human Factors and Ergonomics in Dye Penetration and Magnetic Particle Non-destructive Inspection Methods, City University of Hong Kong, Volume 15, August 2007, EL_15_1_25.

[34]. M. Willcox, G. Downes, A Brief Description of NDT Techniques, Insight NDT Limited, 2000-2003.

[35]. M. Van Dalen, C. Wicker and G. J. Wilson. Non Destructive Testing of Materials Subjected to Atmospheric Stress Corrosion Cracking. 17th World Conference on Non-destructive Testing, Shanghai, China, October 2008, Johannesburg, South Africa.

[36]. International Atomic Energy Agency, Training Guidelines in Non-destructive Testing Techniques: Leak Testing at Level 2, IAEA Training course series no. 52, Vienna International Centre, 2012, ISSN 101-5518.

[37]. M. Sharon, M. Bentzley and R. Goodwin, Basic Principle of Liquid Penetrant Inspection, NDT Liquid Penetrant Testing, November, 2010.

[38]. M. Berke, Non-destructive Material Testing with Ultrasonic, Introduction to basics. 2011.

[39]. L. Tomasz, Studies on Ultrasonic Non-destructive Methods in Inspection of Steel, D.Phils. Dissertation: Uppsala University, 2012.

[40]. American Society for Testing and Material International. SA-388/SA-388M. Standard Practice for Ultrasonic Examination of Heavy Steel Forgings. ASTM Int'l, 2005.

[41]. International Atomic Energy Agency. A Guidebook for Industrial Management and Quality Control Personnel, IAEA Training course series no. 9, Austria: Vienna International Centre, 1999.

[42]. L. Olivier, D. Francois, B. Bernard, Simulation of the probability of defection of flat-bottom hole within a pipe using ultrasounds. ECNDT, 2014.

[43]. M. Crockett. Predictive Maintenance BRO Activities. AEP Plant Engineering Programs, 2009.

[44]. G. S. Reza, D. Yuxia, P. Kira and M. Xavier. Inspection of Glass Fibre Reinforced Plastic using Near Short Wave Infrared and Ultrasound/Optical Excitation Thermography. Smart Material, Structures and NDT in Aerospace. Montreal, Quebec, Canada, 2-4 November 2011.

[45]. I.C. Clemente, Studies on Quantitative subsurface defect evaluation by pulsed phase thermography. Ph.D. Thesis: Laval University Quebec, 2005.

[46]. M. Goldmmer, H. Mooshofer, M. Rothenfusser, J. Bass and J. Vrana. Automated Induction Thermography of Generator Components. Review of Quantitative Nondestructive Evaluation, 2010, Vol. 29, p. 451 - 457.

[47]. B. Patrick, L. Gregory and W. Henri. Comparison between Induction Thermography And Conventional NDT Methods for Forged Parts. *In Proceedings of 11th European* Conference on Non-Destructive Testing (ECNDT 2014). Prague, Czech Republic on 6 - 10 October 2014.

[48]. N. Tsopelas, N.J. Siakavellas. Experimental Evaluation of Electromagnetic Thermal Non-destructive Inspection by Eddy Current Thermography in Square Aluminum Plates. NDT&E International, 2011, 44, p(609-620).

[49]. S. Maillard, J. Cadith, P. Bouteille, G. Legros, J.L. Bodnar, and V. Detalle. Non-destructive testing of forged metallic materials by active infrared thermography. *International Journal of thermophysics*, 2012, pp.1-7.

[50]. R. Yang, Y. He, Logarithmic Analysis of Eddy Current Thermography based on Logitudinal Heat Condition for Subsurface Defect Evaluation. Infrared Physics & Technology, Volume 67, September 2014, p (467-472).

[51]. L. Jia, T. Gui Yun, G. Bin, R. WenWei, M. Jin Song. Investigation of Thermal Imaging Sampling Frequency for Eddy Current Pulse Thermography. NDT&E International, November 2014, 62, p (85-92).

[52]. J. Peng, G. Yun Tian, L. Wang, Y. Zhang, K. Li, X. Gao, Investigation into eddy

current pulsed thermography for rolling contact fatigue detection and characterization, NDT&E International, Volume 74, May 2015, Pages 72-80, ISSN 0963-8695.

[53]. N. Udo and W. Gunter. Induction Thermography as a Tool for Reliable Detection of Surface Defects in Forged Components. 17th World Conference on Non-destructive Testing, Shanghai, China, October 2008, Saarbrucken, Germany.